



Leaky Ca²⁺ release channel/ryanodine receptor 2 causes seizures and sudden cardiac death in mice

Stephan E. Lehnart,¹ Marco Mongillo,¹ Andrew Bellinger,¹ Nicolas Lindegger,² Bi-Xing Chen,¹ William Hsueh,³ Steven Reiken,¹ Anetta Wronska,¹ Liam J. Drew,¹ Chris W. Ward,⁴ W.J. Lederer,^{5,6} Robert S. Kass,² Gregory Morley,³ and Andrew R. Marks^{1,7}

¹Department of Physiology and Cellular Biophysics, Clyde and Helen Wu Center for Molecular Cardiology, and ²Department of Pharmacology, Columbia University College of Physicians and Surgeons, New York, New York, USA. ³The Leon H. Charney Division of Cardiology, New York University School of Medicine, New York, New York, USA. ⁴School of Nursing and ⁵Department of Physiology, University of Maryland, Baltimore, Maryland, USA. ⁶Medical Biotechnology Center, University of Maryland Biotechnology Institute, Baltimore, Maryland, USA. ⁷Department of Medicine, Columbia University College of Physicians and Surgeons, New York, New York, USA.

The Ca²⁺ release channel ryanodine receptor 2 (RyR2) is required for excitation-contraction coupling in the heart and is also present in the brain. Mutations in RyR2 have been linked to exercise-induced sudden cardiac death (catecholaminergic polymorphic ventricular tachycardia [CPVT]). CPVT-associated RyR2 mutations result in “leaky” RyR2 channels due to the decreased binding of the calstabin2 (FKBP12.6) subunit, which stabilizes the closed state of the channel. We found that mice heterozygous for the R2474S mutation in *Ryr2* (*Ryr2*-R2474S mice) exhibited spontaneous generalized tonic-clonic seizures (which occurred in the absence of cardiac arrhythmias), exercise-induced ventricular arrhythmias, and sudden cardiac death. Treatment with a novel RyR2-specific compound (S107) that enhances the binding of calstabin2 to the mutant *Ryr2*-R2474S channel inhibited the channel leak and prevented cardiac arrhythmias and raised the seizure threshold. Thus, CPVT-associated mutant leaky *Ryr2*-R2474S channels in the brain can cause seizures in mice, independent of cardiac arrhythmias. Based on these data, we propose that CPVT is a combined neurocardiac disorder in which leaky RyR2 channels in the brain cause epilepsy, and the same leaky channels in the heart cause exercise-induced sudden cardiac death.

Introduction

Pharmacological seizure models have implicated abnormalities in intracellular Ca²⁺ cycling of inhibitory interneurons and/or astrocytes as a mechanism of seizure generation (1, 2), and the inositol 1,4,5-trisphosphate receptor (IP3R), an intracellular calcium release channel on the ER, has been associated with seizures in mice (3). However, a causal relationship between defective intracellular calcium release channels and seizures has not been reported. Calcium stored within the ER contributes to neuronal signaling and is controlled by intracellular Ca²⁺ release channels, in particular ryanodine receptors (RyRs) (4–6) and IP3Rs (7, 8). To explore the underlying mechanism for seizures in CPVT we generated mice that harbor a missense mutation (RyR2-R2474S) that has been linked to exercise-induced cardiac arrhythmias in humans (9–12).

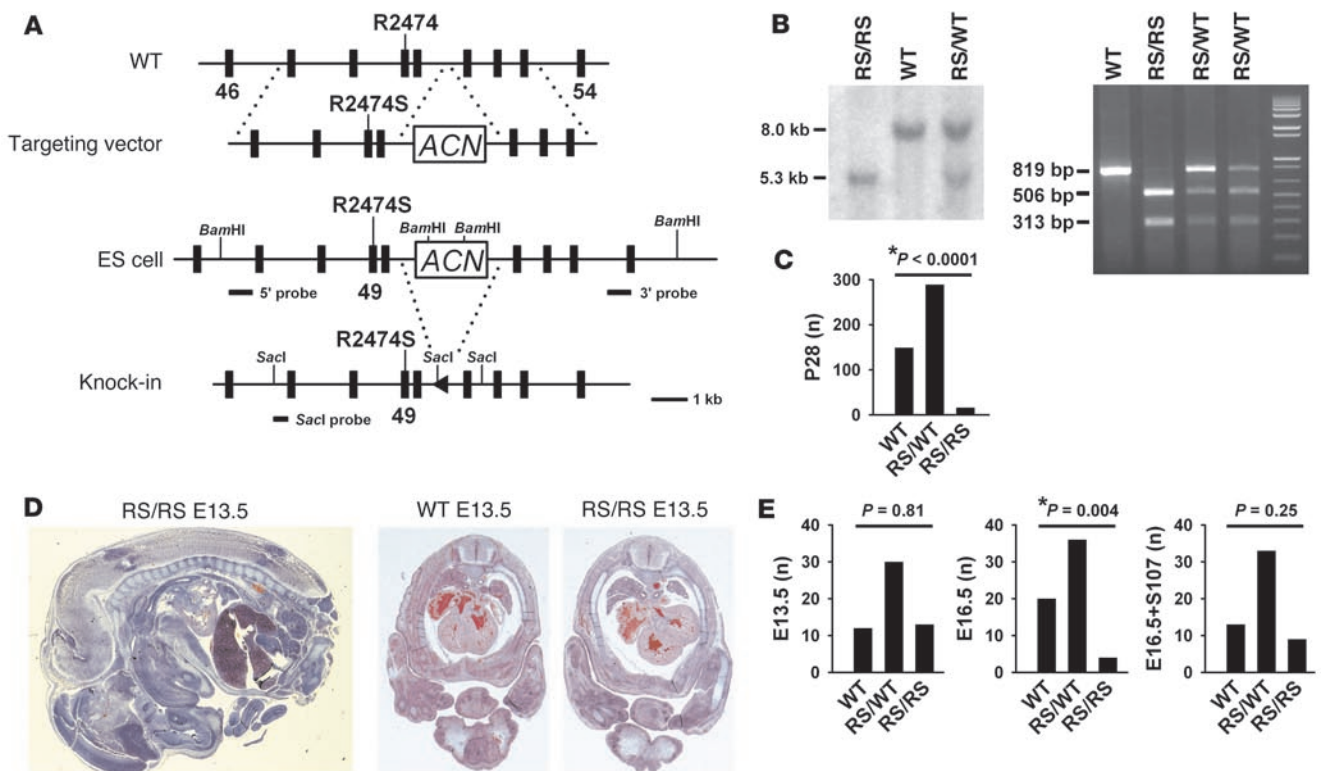
More than 50 distinct *RYR2* mutations have been linked to catecholaminergic polymorphic ventricular tachycardia (CPVT), an arrhythmogenic cardiomyopathy (13–15). CPVT patients experience syncope and sudden cardiac death (SCD) from the toddler to adult ages, and by 35 years age the mortality is up to 50% (13, 16, 17).

Nonstandard abbreviations used: AP, action potential; 4-AP, 4-aminopyridine; CAF, caffeine; CPVT, catecholaminergic polymorphic ventricular tachycardia; DAD, delayed afterdepolarization; IP3R, inositol 1,4,5-trisphosphate receptor; ISO, isoproterenol; *I_{T1}*, transient inward current; NE, norepinephrine; *P_o*, open probability; RyR2, ryanodine receptor 2; SCD, sudden cardiac death; SR, sinus rhythm; sVT, sustained polymorphic VT; VT, ventricular tachycardia.

Conflict of interest: A.R. Marks and S. Reiken are consultants for a start-up company, ARMGO Pharma Inc., that is targeting RyR2 to prevent sudden cardiac death.

Citation for this article: *J. Clin. Invest.* 118:2230–2245 (2008). doi:10.1172/JCI35346.

In the initial clinical descriptions, approximately half of the children with CPVT were reported to present with seizures, including loss of consciousness, convulsions, and involuntary incontinence, “leading to the potential misdiagnosis of epilepsy” (18). Strikingly, approximately 50% of *RYR2* mutation carriers in a large Dutch cohort presented with seizures (19). Additionally, *CASQ2* mutation carriers with CPVT also exhibit seizures (20). RyR2 is highly expressed in the brain, particularly in the dentate gyrus of the hippocampus (Supplemental Figure 3; supplemental material available online with this article; doi:10.1172/JCI35346DS1) and other areas that have been associated with generalized tonic-clonic seizure activity (21). Therefore, we hypothesized that mutant defective (leaky) RyR2 channels could be the cause of neuronal seizures in patients diagnosed with CPVT. Here, we report that generalized tonic-clonic seizures do indeed occur in a knock-in mouse model of a *RYR2* missense mutation (R2474S) found in CPVT patients (22) and provide evidence supporting a causal role for leaky RyR2 channels in both epilepsy and fatal ventricular arrhythmias, showing that a novel RyR-specific drug, S107 (23), which prevents a leak in the channel but does not block the channel or alter normal Ca²⁺ signaling, is able to inhibit both seizures and arrhythmias in the mutant mice (see supplemental data for S107 structure and accompanying information on the drug, which is a novel, orally available 1,4-benzothiazepine derivative with high RyR2 activity and no significant off-target effects). Taken together, our findings suggest that an RyR2-mediated intracellular Ca²⁺ leak contributes to defective neuronal and cardiac excitability that trigger seizures and cardiac arrhythmias.

**Figure 1**

RyR2-homozygous R2474S knock-in mice exhibit increased embryonic lethality that is reduced by a novel RyR2 stabilizing drug (S107) that inhibits Ca^{2+} leak. **(A)** Generation of *Ryr2*-R2474S knock-in mouse. Top: targeted mutagenesis of mouse RyR2 exon 49; middle: homologous ES cell recombination of the mutant *Ryr2*-R2474S allele; bottom: Cre-mediated excision of the floxed *neo* cassette results in *Ryr2*-R2474S knock-in. **(B)** Confirmation of homologous recombination of mutant *Ryr2*-R2474S allele by Southern blot (left); PCR detects mutant R2474S (RS) allele in progeny (right). **(C)** Lethality of the homozygous *Ryr2*-R2474S (RS/RS) mice at day 28 after birth as evidenced by significant non-Mendelian inheritance with underrepresentation of the homozygous genotype. **(D)** Normal embryonic development and cardiac maturation up to day E13.5 as shown by representative histological sections. Original magnification: $\times 3$ (left, longitudinal section), $\times 5$ (right, cross-sections). **(E)** Rescue of homozygous *Ryr2*-R2474S embryos by treatment of the pregnant mothers with S107, a small compound that binds specifically to RyR2, enhances calstabin2 binding and inhibits Ca^{2+} leak from mutant RyR2 channels. Up to day E13.5, there was normal Mendelian inheritance (left). However, embryonic lethality was evidenced by abnormal Mendelian inheritance at day E16.5 (middle), and this was prevented by S107 treatment, which resulted in normal Mendelian inheritance due to improved survival of the homozygous *Ryr2*-R2474S embryos (right). *P* values represent statistical comparison of the observed genotypes to expected genotypes based on Mendelian inheritance patterns. Asterisks indicate significant difference between the observed and expected genotype ratios.

Results

Heterozygous *RYR2* missense mutations have been found in patients with CPVT and cohorts with sudden unexpected death (15). CPVT-linked *RYR2* mutations are clustered in 3 disease-susceptible regions of the channel (24, 25). One mutation cluster occurs in the central *RYR2* region and includes an *RYR2*-R2474S missense mutation originally described in identical twin brothers with syncope and exercise-induced ventricular tachycardia (VT) (13). Previously, we reported a gain-of-function defect in PKA-phosphorylated *Ryr2*-R2474S channels coexpressed with calstabin2 under conditions of low activating $[\text{Ca}^{2+}]$ to simulate cardiac diastole (the period in the cardiac cycle when arrhythmic triggers known as delayed afterdepolarizations [DADs] occur) during exercise (22). We showed that the *Ryr2*-R2474S mutant channels and 3 other CPVT-linked mutant RyR2 channels all exhibited a leaky phenotype under conditions that simulate cardiac diastole during exercise. This defective channel function was due to decreased binding of calstabin2 resulting in a shift to the left of the Ca^{2+} dependence of RyR2 activation such

that these channels, unlike WT controls, were capable of being activated at extremely low (i.e., ~ 150 nM) cytosolic $[\text{Ca}^{2+}]$. We interpreted these findings as being consistent with the generation of diastolic SR Ca^{2+} leak via mutant RyR2 channels in the heart that could trigger arrhythmias during exercise.

To examine the role of leaky RyR2 channels in vivo, we generated knock-in mice carrying the missense mutation R2474S in the endogenous *Ryr2* gene (*Ryr2*^{RS/WT}; see Figure 1A and Methods). The targeting vector for homologous recombination consisted of genomic DNA spanning a region that includes introns 46–54, with the codon change resulting in the R2474S variant occurring in exon 49. Homologous recombination was confirmed in ES cells using BamHI digestion (Figure 1B). Following germline transmission and mating of chimeras with 129Sv females, offspring were backcrossed into the C57BL/6 background for at least 5 generations, in agreement with previous arrhythmia studies in mice (26). Importantly, RyR2 expression was not different in the heart and brains of *Ryr2*-R2474S mice compared with WT littermate controls.



Heterozygous *Ryr2*-R2474S/WT (*Ryr2*^{RS/WT}) mice were viable and survived into adulthood. However, *Ryr2*-R2474S knock-in mice were not born at the expected Mendelian ratios: observed/expected genotype ratios at weaning age were *Ryr2*^{WT/WT}, 149/113.5 (32.8%); *Ryr2*^{RS/WT}, 289/227 (63.6%); *Ryr2*^{RS/RS}, 16/113.5 (3.5%); $P < 0.0001$ ($\chi^2 = 111.7$; Figure 1C). This result is in agreement with the fact that all previously identified *RYR2* mutation carriers are heterozygous (individuals homozygous for CPVT-linked *RyR2* mutations have not been reported) (15). The selective loss of homozygous *Ryr2*^{RS/RS} embryos occurred due to increased intrauterine lethality. Indeed, homozygous *Ryr2*^{RS/RS} mating did not produce any offspring from confirmed impregnated female mice, indicating intrauterine lethality of the *Ryr2*^{RS/RS} genotype ($n = 6$).

RyR2 channels are first detected in the heart at day E8.5 in mice (27). Histology confirmed normal intrauterine development of homozygous *Ryr2*^{RS/RS} mice until E13.5. In particular, cardiac maturation, chamber development, and circulation appeared to be normal at E13.5, as evidenced by transverse embryonic sections through the heart region (Figure 1D). While the expected Mendelian distribution was observed at E13.5, at E16.5 embryonic genotypes deviated significantly from the expected Mendelian distribution, consistent with an increased number of growth-retarded or digested *Ryr2*^{RS/RS} E16.5 embryos due to intrauterine death (Figure 1E). Homotetrameric *RyR2* channels comprising 4 CPVT mutant subunits exhibited a significantly greater gain-of-function defect as compared with heterotetrameric *RyR2* channels (22), which is consistent with the fact that heterozygous *Ryr2*^{RS/WT} mice did not show increased intrauterine mortality. To test the hypothesis that the intrauterine death observed in *Ryr2*^{RS/RS} mice was due to defective *RyR2* channel function (i.e., Ca^{2+} leak), we used a novel, *RyR*-selective 1,4-benzothiazepine derivative, S107 (23), that stabilizes *RyR2* channels by enhancing the binding affinity of calstabin2 to mutant and/or PKA-phosphorylated channels. S107 is a small (MW, 245.7) compound that enhances calstabin2 binding to *RyR2* at low nanomolar concentrations and failed to interact with over 400 receptors, enzymes, and ion channels in screens using up to 10 μM of the compound (see supplemental data). Specifically, S107 had no effect on cardiac ion channels including the voltage-gated Na^+ , K^+ , and Ca^{2+} channels at concentrations up to 10 μM , and S107 had no effect on normal Ca^{2+} signaling in cells. We reasoned that if the defective *RyR2* function was causing late intrauterine death in *Ryr2*^{RS/RS} mice, then S107 might prevent the excess *Ryr2*^{RS/RS} mortality observed at E16.5. Indeed, we found that treatment of *Ryr2*^{RS/WT} mothers with S107 (5 mg/kg s.c. continuously by osmotic minipump for 14 days) resulted in rescue of the expected Mendelian distribution at E16.5 (Figure 1E). On the basis of these data, we concluded that the likely cause of intrauterine mortality at E16.5 is excess Ca^{2+} leak via mutant defective *RyR2* channels in *Ryr2*^{RS/RS} mice.

Ryr2^{RS/WT} mice began to exhibit spontaneous seizures during the weaning period between P21 and P28. There were no obvious developmental abnormalities, and the brains were histologically normal in *Ryr2*-R2474S mice (see supplemental data). The seizures were spontaneous and recurrent, and their frequency (1–3/week) did not change during a 3-month observation period (e.g., Supplemental Video 1). Generalized tonic-clonic seizures in *Ryr2*^{RS/WT} heterozygous mice occurred following mouse placement in a new cage and/or arousal from sleep; however, seizures also occurred in the absence of these environmental changes (see Supplemental Video 1). Seizures exhibited a progression through several stages.

Following an initial state of reduced activity and lying flat on the cage floor, the mice typically exhibited several behavioral signs of seizure activity (grimacing, ear deflection, nose hair stiffening, Straub tail, head bobbing), which quickly progressed from partial, isolated limb jerking to sustained and violent generalized myoclonic jerking. Following a generalized myoclonic phase, *Ryr2*^{RS/WT} mice developed outstretched hind limbs consistent with tonic-clonic seizures, bilateral forelimb clonus, and head bobbing. The entire sequence of seizure activity typically lasted for 20–120 seconds, and both clonic and tonic-clonic seizures were recorded; this was followed by the mouse freezing and then resting for several minutes (corresponding to the postictal state). We were able to capture several spontaneous, generalized seizures by EEG recording, which confirmed the generalized nature of the seizures. Overall, spontaneous seizures were directly observed in 23 of 50 heterozygous *Ryr2*^{RS/WT} and 2 of the very few homozygous *Ryr2*^{RS/RS} mice surviving into adulthood but never in WT mice; however, it is likely that the actual incidence of seizures was higher than observed, because it was not possible to observe all of the mice constantly, and 100% of the mutant mice exhibited lowered thresholds for pharmacologic-induced seizures compared with WT littermate controls (see below).

Heterozygous *Ryr2*^{RS/WT} mice with confirmed recurrent generalized seizures were implanted with cortical EEG electrodes and ECG telemeters and monitored during a 4-week period. Following electrode placement, spontaneous epileptiform activity was never observed in freely moving WT mice, which showed regular cardiac sinus rhythm (SR) ($n = 3$; e.g., Figure 2A). Similarly, heterozygous *Ryr2*^{RS/WT} mice exhibited normal periods of low-amplitude baseline cortical EEG and regular SR activity ($n = 4$; e.g., Figure 2B). EEG monitoring from 2 heterozygous *Ryr2*^{RS/WT} mice confirmed the occurrence of spontaneous electrographic and behavioral seizures, consistent with epileptiform ictal activity (Figure 2C). In agreement with video-documented behavioral abnormalities (see Supplemental Video 1), EEG rapid spike discharges during generalized tonic-clonic seizures typically lasted for 20–30 seconds. Moreover, slower spike discharges were observed in the postictal period (Figure 2D).

Since seizures in CPVT mutation carriers have been attributed to malignant arrhythmias causing rapid compromise of cerebral blood supply (Stokes-Adams attacks) (18), we performed simultaneous ECG-EEG recording. During spontaneous tonic-clonic seizures with ictal EEG spike activity, mice displayed regular fast SR (sinus tachycardia, $\sim 690/\text{min}$); however, no peri-ictal arrhythmias were ever observed (Figure 2C, ECG-EEG). Our data show that spontaneously recurring seizures in heterozygous *Ryr2*^{RS/WT} mice are due to abnormal brain excitability and are not associated with loss of consciousness (syncope) occurring from arrhythmias (i.e., the seizures are not Stokes-Adams attacks).

Since it was not possible to accurately assess the incidence of spontaneous seizures in *Ryr2*-R2474S mice, we sought to compare seizure susceptibility in WT and *Ryr2*^{RS/WT} mice using pharmacological testing. Intraperitoneal administration of 4-aminopyridine (4-AP) has been reported to cause generalized tonic-clonic seizures and a prototypical progression of epileptic seizure activity in rodents (28). To enable quantitative examination of seizure susceptibility in the mice, we administered 4-AP (2.5 mg/kg i.p.) and the *RyR* agonist caffeine (CAF; 250 mg/kg i.p., administered 25 minutes after 4-AP), following which generalized tonic-clonic seizures (stage 3) occurred significantly earlier in *Ryr2*^{RS/WT} mice

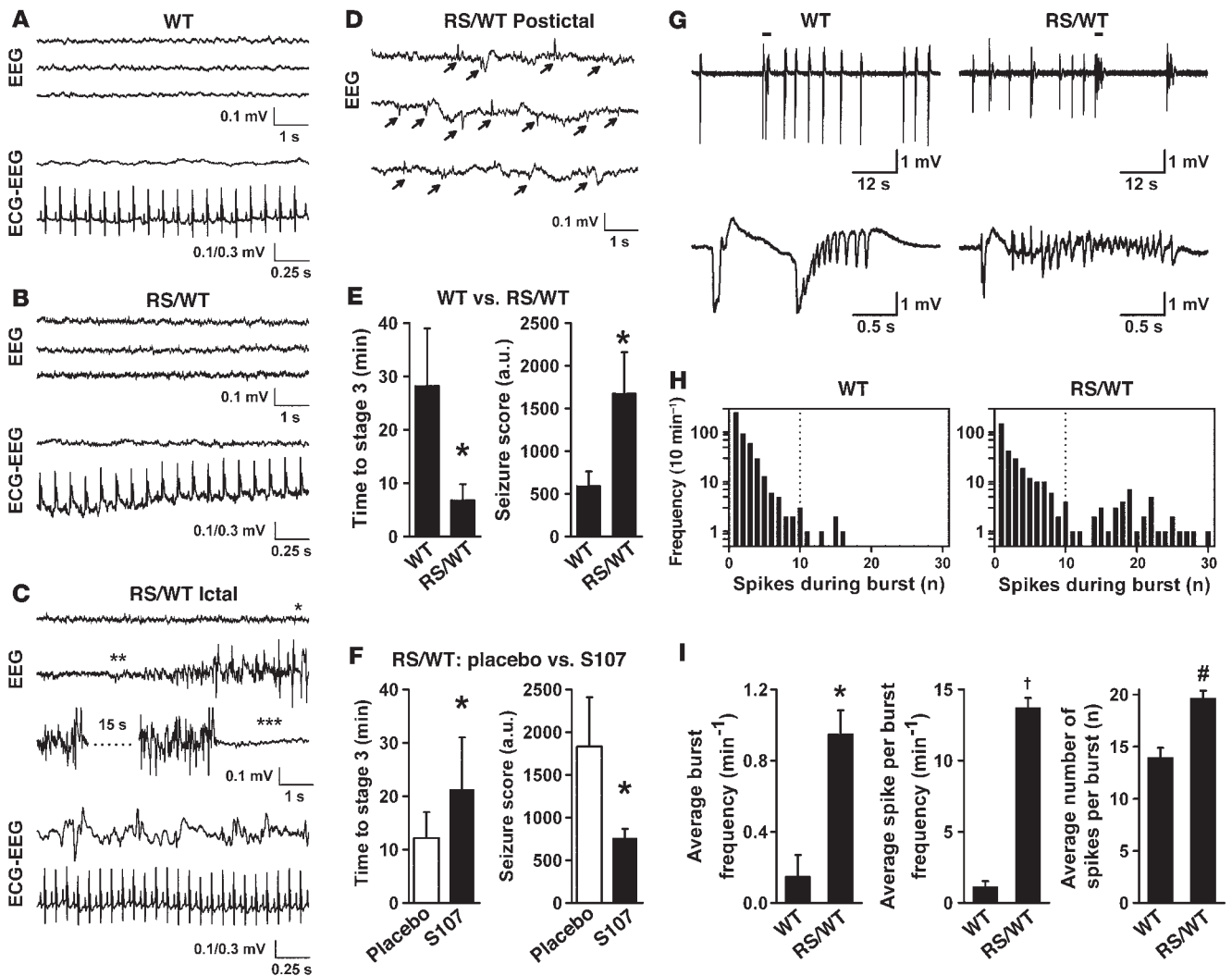


Figure 2

Epileptic seizures in heterozygous *Ryr2^{RS/WT}* mice are inhibited by prevention of the leak via RyR2 channels. (A) Representative EEG and simultaneous ECG (ECG-EEG) recordings from a WT littermate mouse, showing normal brain activity and a normal cardiac SR; and (B) a heterozygous *Ryr2^{RS/WT}* mouse during an interictal period without epileptiform activity, showing normal brain activity and a normal sinus heart rhythm. (C) Recordings from an *Ryr2^{RS/WT}* mouse during an ictal episode, showing abnormal EEG activity but a normal cardiac rhythm (sinus tachycardia). The recorded seizure began with the Straub tail sign (single asterisk), followed by generalized tonic-clonic seizure (double asterisks), then spiking activity that gradually increased in amplitude and rhythmicity and ended with a depressed electric postictal period characterized by relaxed muscle tone, indicating end of seizure (triple asterisks). Consecutive 8-second traces from one EEG channel (left hemisphere) are shown; there was no difference in the spiking patterns between the left and right hemispheric activity; and (D) EEG recording during a postictal period with epileptiform activity (arrows). (E) Average latency to development of generalized tonic-clonic seizures and overall seizure score comparison in WT and *Ryr2^{RS/WT}* mice following 4-AP and CAF susceptibility testing. **P* < 0.05. (F) Average latency to development of generalized tonic-clonic seizures and overall seizure score comparison in *Ryr2^{RS/WT}* mice treated with S107 subjected to a seizure protocol identical to that in E, showing that S107 partially protects against seizures. **P* < 0.03 (left); **P* < 0.04 (right). (G) Morphology of seizure-like events recorded from CA3 region of hippocampal slices incubated in 10 μM 4-AP from WT (*n* = 4) and *Ryr2^{RS/WT}* (*n* = 4) mice shown at low and high time resolution. Short bars above traces indicate portion of recording that is expanded in the lower traces. (H) Histogram analysis of number of spikes per burst, showing longer bursts in the *Ryr2^{RS/WT}* compared with WT mice. (I) Bar graphs showing analyses of complex burst activity only (defined as more than 10 spikes per burst, consistent with seizure-like activity). Left: Frequency per minute of complex bursts; middle: frequency of spikes per minute per complex burst; right: average number of spikes per complex burst, all of which were significantly elevated in *Ryr2^{RS/WT}* compared with WT mice. **P* < 0.005; †*P* < 0.0001, #*P* < 0.001.

(*n* = 5) compared with WT (Figure 2E, left; *n* = 5, *P* < 0.05). Moreover, in *Ryr2^{RS/WT}* mice, combined 4-AP and CAF treatment resulted in faster progression to a significantly higher seizure severity score, including death (Figure 2E, right). To further determine whether the observed seizure activity was in fact due to defective

RyR2 channel function, we tested whether treatment with S107, which inhibits Ca²⁺ leak via mutant RyR2 channels, could protect against seizures in the *Ryr2-R2474S* heterozygous mice. Pretreatment for 1 week with S107 (5 mg/kg/h via s.c. osmotic pump) significantly increased the latency time for developing seizures and

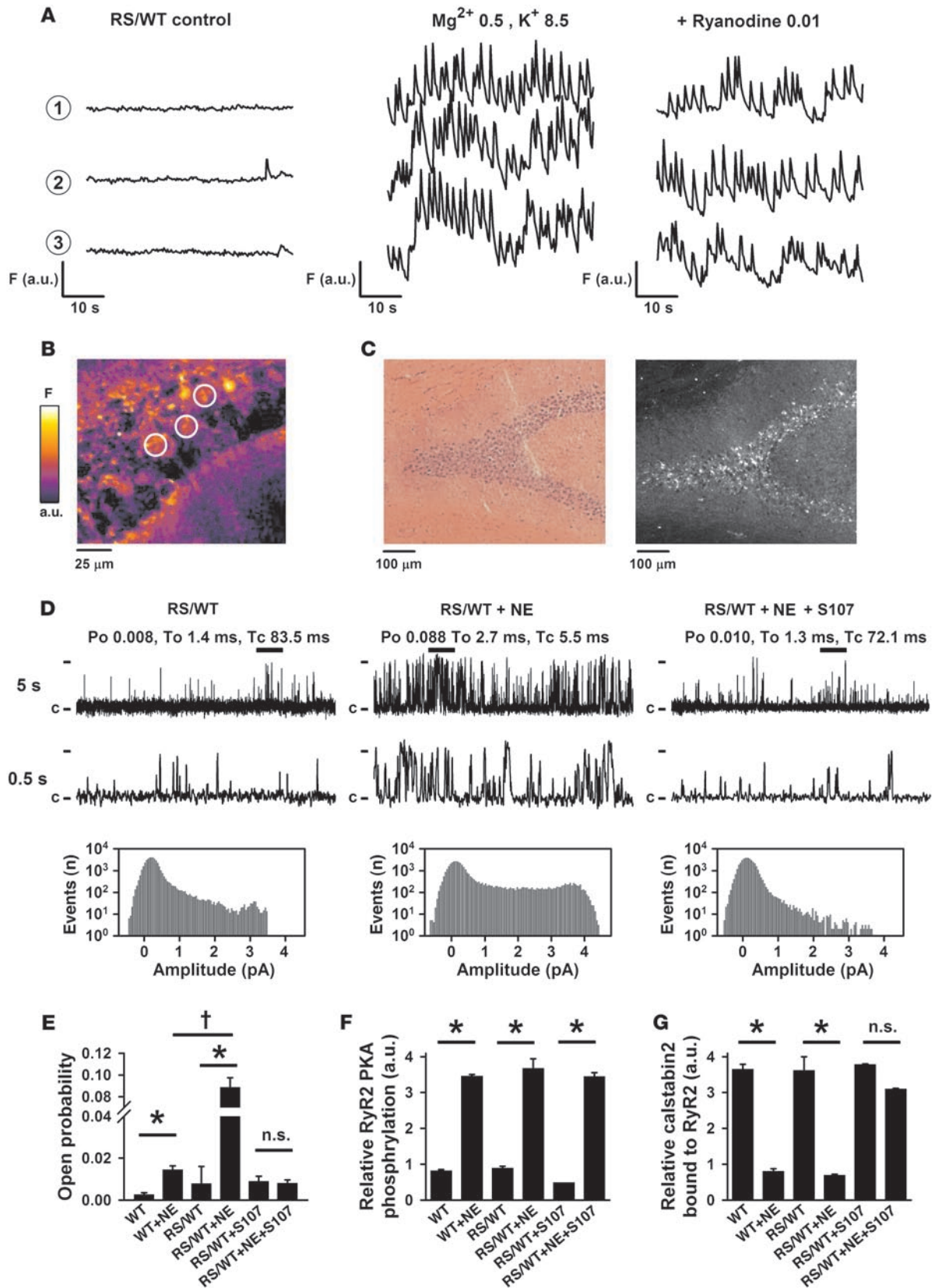




Figure 3

Hippocampal *Ryr2^{RS/WT}* brain slices and channels exhibit burst activity, which can be inhibited by treatment with ryanodine or the RyR-stabilizing drug S107, respectively. (A and B) Continuous confocal Ca²⁺ fluorescence imaging of the *Ryr2^{RS/WT}* CA3 principal cell layer under control conditions (left), and seizure activity induced by low Mg²⁺ (0.5 mM) plus high K⁺ (8.5 mM) (middle) and following ryanodine (10 μM) treatment (right). Fluorescence (F) signals 1–3 in A correspond to regions of interest indicated by white circles in the CA3 layer in B. Data are representative of 3 experiments using *Ryr2^{RS/WT}* hippocampal slices; dimensions are as indicated. (C) H&E histology (left) and RyR2 immunohistochemistry (right) of the hippocampal CA3 region in *Ryr2^{RS/WT}* brain slices show increased RyR2 expression in the preserved principal cell layer. There were no histological abnormalities compared with WT (data not shown). (D) Representative *Ryr2^{RS/WT}* single-channel traces from vesicles of isolated hippocampus from sedentary mice (left), after injection of NE (5 mg/kg twice over 3 hours; middle) or after 1 week treatment with S107 (5 mg/kg/h) followed by NE treatment (5 mg/kg twice over 3 hours; right). P_o, mean open (To) and mean closed (Tc) times, closed state (c), and the fully open level (4 pA) are indicated. Thick bars above the 5-second traces indicate area shown at higher resolution in the 0.5-second traces. All-point histograms corresponding to the single-channel traces show increased numbers of partial openings (subconductance states) and overall increased activity of the brain channels from NE-treated *Ryr2^{RS/WT}* mice (middle histogram). The histogram on the right shows more channels in the closed state (0 pA), consistent with the channel-stabilizing properties of the drug S107 that enhances binding of the calstabin2 subunit to the channel. (E) Average P_o of WT and *Ryr2^{RS/WT}* brain channels under different treatment conditions as indicated. Single-channel measurements were performed at a *cis* (cytosolic) Ca²⁺ concentration of 150 nM. *P < 0.05 versus NE-untreated; †P < 0.05, NE-treated WT versus *Ryr2^{RS/WT}*. Each bar represents the average of 7–9 channels. Equivalent amounts of RyR2 were immunoprecipitated from brain homogenates with an RyR2 isoform-specific antibody followed by immunoblotting; bar graphs show the amount of PKA phosphorylation of RyR2 at Ser2808 (F) and the amount of calstabin2 bound to RyR2 (G) under the indicated conditions. Animals were treated with S107 via implantable osmotic pumps (5 mg/kg/h) for 7 days before NE stimulation. *P < 0.05 versus NE-untreated.

reduced the seizure score in the *Ryr2-R2474S* heterozygous mice (vehicle-treated *Ryr2^{RS/WT}*, n = 7; S107-treated *Ryr2^{RS/WT}*, n = 10; P < 0.03 for latency time and P < 0.04 for seizure score; Figure 2F).

Certain behavioral aspects of the characteristic epileptiform activity in *Ryr2^{RS/WT}* mice are indicative of a hippocampal seizure origin in rodent epilepsy models. To explore this possibility, we performed extracellular local field potential (LFP) recordings in the CA3 region of hippocampal brain slices that were exposed to 4-AP (10 μM). *Ryr2^{RS/WT}* hippocampal slices (n = 4) exhibited significantly increased excitability in response to 4-AP, as evidenced by a significantly higher frequency of more-complex interictal burst discharges (>10 spikes/burst), higher spike rates per burst, and higher spike numbers per complex burst (n = 4; Figure 2, G–I). When population burst discharge activity following 4-AP treatment (10 μM) over 10 minutes was compared in WT (n = 488 events analyzed) and *Ryr2^{RS/WT}* slices (n = 322 events analyzed), a significant shift toward longer and faster burst activity consistent with a second peak in the event distribution was evident (Figure 2H). The observed increase in 4-AP-induced complex burst activity in the *Ryr2^{RS/WT}* compared with WT hippocampal CA3 region suggests that the seizure activity in the *Ryr2^{RS/WT}* mice may originate in the hippocampus.

To determine whether the mechanism of the seizures observed in *Ryr2^{RS/WT}* mice involves aberrant Ca²⁺ signaling in the hippocampal CA3 region, we performed confocal Ca²⁺ imaging experiments using hippocampal brain slices (n = 3). During perfusion with a low-Mg²⁺ (0.5 mM) and high-K⁺ (8.5 mM) solution, cells in the principal hippocampal CA3 layer (Figure 3B) exhibited profound burst activity compared with quiescent cells under control conditions (Figure 3A, left vs. middle) or cells from WT (n = 4) mice hippocampal brain slices examined under the same conditions (data not shown). Moreover, addition of the specific RyR channel blocker ryanodine (10 μM) reduced the amplitude and frequency of the burst activity, suggesting that leaky *Ryr2^{RS/WT}* activity likely contributes to Ca²⁺-dependent burst activity (Figure 3A, right). Histological examination of the WT and *Ryr2^{RS/WT}* mouse brains using H&E staining (e.g., Figure 3C, left; n = 5 *Ryr2^{RS/WT}* brains, n = 5 WT brains) and trichrome staining (data not shown) did not reveal any abnormalities in the hippocampal formation or other brain areas of *Ryr2^{RS/WT}* mice, and RyR immunostaining confirmed normal RyR2 expression, particularly in the CA3 region (e.g., Figure 3C, right; see also Supplemental Figure 3). These data indicate that the increased susceptibility to seizure-like activity *in vitro* and generalized seizures *in vivo* are likely associated with high-frequency Ca²⁺ signaling and/or burst activity.

To further characterize the molecular mechanisms that may contribute to abnormal cellular Ca²⁺ signals, we studied native RyR channels harvested from the isolated mouse hippocampus. RyR2 Ca²⁺ release channels comprise 4 RyR2 monomers, each of which binds a single calstabin2 subunit (also known as FKBP12.6), which stabilizes the channel closed state (22, 29). We have previously found significantly increased channel activity and calstabin2 depletion in recombinant homotetrameric *Ryr2-R2474S* as well as in heterotetrameric *Ryr2-WT/R2474S* channels following *in vitro* PKA phosphorylation (22). Since activation of noradrenergic stimulation can result in epileptic synchronization and altered hippocampal activity (30), we treated *Ryr2^{RS/WT}* and WT littermates with norepinephrine (NE; 5 mg/kg/h s.c. by osmotic pump for 48 hours) and measured RyR single-channel activity from brain vesicles fused to planar lipid bilayers. The open probability (P_o) of hippocampal RyR channels was significantly increased in NE-treated compared with untreated *Ryr2^{RS/WT}* mice (Figure 3, D and E). Current amplitude histograms at 150 nM *cis* Ca²⁺ were consistent with increased P_o including multiple subconductance states, suggesting a leaky channel phenotype (Figure 3D, middle). Given that 3 RyR isoforms are expressed throughout the brain, we could not be sure that the channels in these single-channel recordings were RyR2; however, RyR2 is the most abundant isoform in the hippocampus (the exception being cerebellar Purkinje neurons expressing primarily the skeletal muscle RyR1 isoform; see Supplemental Figure 3). As compared with channels from NE-treated WT mouse brains, *Ryr2^{RS/WT}* channels showed a significantly higher average P_o, consistent with a gain-of-function defect (Figure 3E; n = 9, P < 0.05). Moreover, *Ryr2^{RS/WT}* mice pretreated for 1 week with the RyR2-stabilizing drug S107 showed brain RyR channel activity comparable to that in animals not treated with NE and consistent with normalized function (Figure 3, D and E; n = 9, P < 0.05).

RyR2 immunoprecipitation (using an antibody specific for the RyR2 isoform) from *Ryr2^{RS/WT}* brain homogenates followed by immunoblotting showed no change in RyR2 levels compared with WT (data not shown), and NE treatment resulted in a similar increase in RyR2 PKA phosphorylation in WT and *Ryr2^{RS/WT}* brains

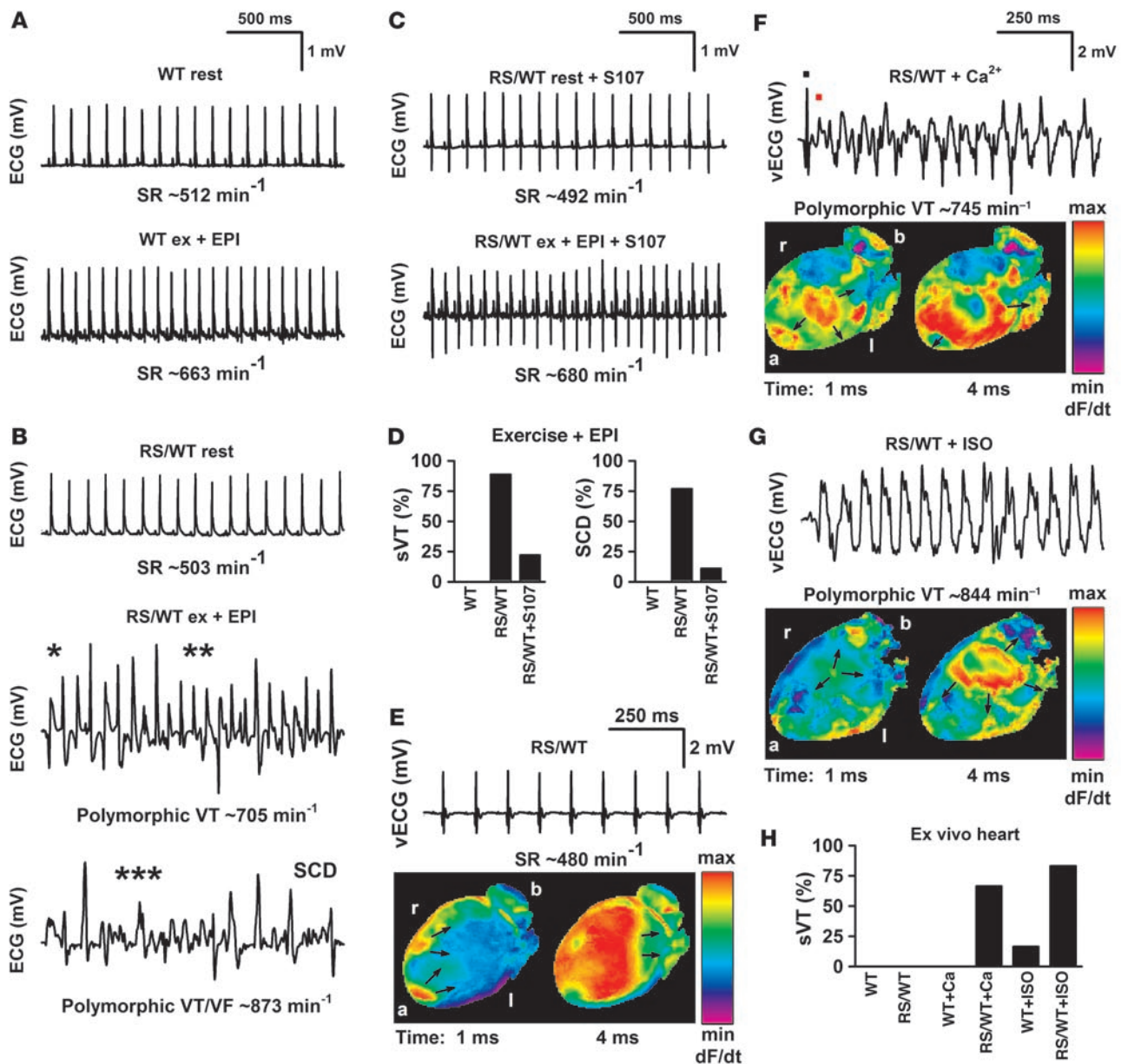


Figure 4

Fixing the leak in mutant channels from *Ryr2^{RS/WT}* mice with S107 protects against fatal cardiac arrhythmias. (A–C) Representative telemetric ECG recordings of WT ($n = 6$), heterozygous *Ryr2^{RS/WT}* ($n = 9$), and *Ryr2^{RS/WT}* mice treated with S107 ($n = 9$). (A) ECGs of a WT mouse, sedentary (rest) and after 45 minutes of treadmill running immediately followed by catecholamine injection (ex + EPI; epinephrine, 0.5 mg/kg i.p.). (B) ECGs of a *Ryr2^{RS/WT}* mouse, sedentary and following arrhythmia provocation stress testing, which resulted in rapid sVT and SCD. *Bidirectional VT; **polymorphic VT; ***rapid polymorphic VT. (C) *Ryr2^{RS/WT}* mice treated with S107 under sedentary housing conditions (rest) and following stress testing (S107, 5 mg/kg/h s.c. for 7 days by osmotic pump). S107 prevented stress-induced arrhythmias. (D) Occurrence of sVT (left) and SCD (right). (E) Example of Langendorff-perfused *Ryr2^{RS/WT}* hearts ($n = 6$) that exhibited regular SR recorded by volumetric ECG (vECG) with 2 epicardial breakthroughs (arrows) and homogenous apical-to-basal voltage activation. (F) Epicardial voltage activation map of the same *Ryr2^{RS/WT}* heart showing multiple activation foci (arrows) and abnormal activation wavefront propagation during rapid polymorphic VT. The black dot marks the last regular sinus beat of vECG, and the red dot the first abnormal beat occurring at a short coupling interval. (G) *Ryr2^{RS/WT}* heart showing abnormal focal activation (arrows) rapidly moving toward apex and left ventricle during sVT. (H) Occurrence of sVT in ex vivo perfused WT and *Ryr2^{RS/WT}* hearts (each $n = 6$). Perfusion in the absence or presence of either high extracellular Ca^{2+} (9 mM) or ISO (100 nM) resulted in sVT in 9 of 12 *Ryr2^{RS/WT}* but only in 1 of 12 WT hearts. Orientation of the heart is as indicated; a, apex; b, base; l, left; r, right of anterior activation maps.



(Figure 3F). Calstabin2 depletion from PKA-phosphorylated RyR2 complexes was significantly increased in both WT and *Ryr2^{RS/WT}* brains following NE stimulation (Figure 3G). When *Ryr2^{RS/WT}* mice were pretreated with the blood brain barrier-permeable S107 compound (5 mg/kg/h s.c. for 1 week) prior to NE treatment, calstabin2 binding to PKA-phosphorylated *Ryr2^{RS/WT}* brain channels was restored to normal levels observed in nonphosphorylated channels (Figure 3G), consistent with single-channel function being normalized (Figure 3D, right). In these experiments, WT RyR1 and RyR3 channels were likely also PKA phosphorylated in mice treated with NE. However, previous studies have shown that despite transient PKA phosphorylation, WT RyR channels do not develop pathologic Ca^{2+} leak that is observed in PKA-phosphorylated CPVT-linked mutant RyR2 channels (16, 22). This is likely due to the finding that the CPVT-linked mutant RyR2 channels bind the stabilizing protein calstabin2 at a lower affinity and are, therefore, more prone to developing a significant, persistent Ca^{2+} leak.

Since telemetric ECG recording of cage-habituated *Ryr2^{RS/WT}* mice did not show any sustained VT leading to syncope or seizures, we performed strenuous exercise stress testing followed by catecholamine injection using previously established protocols (22, 31). WT mice did not exhibit any arrhythmias when this protocol was used (Figure 4A; $n = 6$). Exercise at incrementally faster treadmill speeds for at least 45 minutes followed by epinephrine injection (0.5 mg/kg i.p.) resulted in sustained polymorphic VT (sVT) and SCD in *Ryr2^{RS/WT}* mice (Figure 4B; $n = 8$ of 9). The cardiac arrhythmias in the *Ryr2-R2474S* mice typically started with premature ventricular ectopic beats, progressing into bidirectional and polymorphic VTs (Figure 4B) similar to the stress-induced arrhythmias observed in human RyR2 mutation carriers. These arrhythmias typically degenerated into polymorphic VT and/or fibrillation and finally sudden death. SCD in *Ryr2^{RS/WT}* mice was associated with occasional limb jerking and rapid breathing. However, during or after sVT, none ($n = 0$ of 9) of the *Ryr2^{RS/WT}* mice displayed the sustained generalized tonic-tonic seizures described above (Figure 2; see also Supplemental Video 1). These data further suggest that spontaneous seizures in *Ryr2^{RS/WT}* mice are likely due to epilepsy and are not associated with sustained cardiac arrhythmias.

Using a different CPVT mouse model (calstabin2-deficient mice), we previously showed that VT and SCD could be prevented by pretreatment with JTV519, a 1,4-benzothiazepine (32, 33). Since JTV519 has off-target activity including potent HERG K^+ channel block that can cause drug-induced long QT potentially predisposing to polymorphic VT, we have developed a novel orally available derivative (S107) with higher RyR2 activity and no significant off-target effects (supplemental data, S107 Characterization). Using previously established protocols (32), *Ryr2^{RS/WT}* mice were treated for 1 week with S107 (5 mg/kg/h s.c. by osmotic pump) prior to exercise stress testing. In contrast to untreated *Ryr2^{RS/WT}* mice, of which 8 of 9 exhibited sVT and 7 of 9 had SCD, S107-treated *Ryr2^{RS/WT}* mice subjected to exercise stress testing and low-dose epinephrine injection were less likely to develop sVT (2 of 9) and SCD ($n = 1$ of 9; Figure 4, C and D). Since S107 has high RyR2 specificity and efficacy in vitro, we hypothesized that it may prevent arrhythmias and SCD through an RyR2-targeted mechanism in vivo (see below).

Since a variety of ventricular arrhythmia types have been documented in *RYR2* mutation carriers (34), we sought to determine which form of arrhythmia is associated with SCD (see supplemental data for details). Optical mapping of the ventricular arrhythmias

(Figure 4, E–H) indicated a catecholaminergic and/or intracellular Ca^{2+} overload-dependent mechanism of arrhythmia induction in CPVT hearts, consistent with previous studies (35, 36).

Isolated ventricular cardiomyocytes from *Ryr2^{RS/WT}* hearts were patch-clamped for action potential (AP) recording under current clamp conditions and continuously paced at 1 Hz in control extracellular solution, followed by stimulation with isoproterenol (ISO; 1 μM). In contrast to WT cells (data not shown), ISO-treated *Ryr2^{RS/WT}* cardiomyocytes exhibited DADs between pacing cycles (Figure 5A, asterisks). DADs progressively increased the membrane depolarization rate from 1 Hz (pacing frequency) to approximately 3 Hz (pacing and DADs), and coupling intervals were decreased, resulting in AP fusion, incomplete repolarization, and spontaneous pacemaker activity (automaticity). In many cells, automaticity was self-sustained, e.g., trains of DADs would continue spontaneously after cessation of pacing (data not shown), confirming earlier results from *Ryr2-R4496C* knock-in cells (37). Similarly, ISO-treated *Ryr2^{RS/WT}* cardiomyocytes exhibited aberrant intracellular Ca^{2+} transients (asterisks) between regular field-stimulated Ca^{2+} transients (Figure 5B) that became self-sustained when pacing was stopped, consistent with regenerative intracellular Ca^{2+} release.

We have previously shown that abnormal intracellular Ca^{2+} release from RyR2s in a mouse model of catecholaminergic arrhythmias activates arrhythmogenic transient inward current (I_{TI}) as a mechanism of triggered activity and DADs (33). Accordingly, in ISO-treated *Ryr2^{RS/WT}* cardiomyocytes, we observed I_{TI} events during and immediately following cessation of pacing (e.g., Figure 5C). Control *Ryr2^{RS/WT}* cells without ISO treatment exhibited significantly fewer I_{TI} events, consistent with earlier studies (33) ($n = 6$, $P < 0.05$), and β -adrenergic stimulation of *Ryr2^{RS/WT}* cardiomyocytes resulted in significantly increased cellular I_{TI} density (Figure 5D; $n = 7$, $P < 0.05$). Moreover, treatment of *Ryr2^{RS/WT}* mice with S107 for 1 week significantly decreased I_{TI} density (Figure 5D; $n = 4$, $P < 0.05$). Simultaneous intracellular Ca^{2+} and I_{TI} recording in *Ryr2^{RS/WT}* cardiomyocytes showed that regular pacing-induced Ca^{2+} transients were followed by abnormal intracellular Ca^{2+} release events, which became organized into cell-wide Ca^{2+} waves (Figure 5E, top). Interestingly, arrhythmogenic I_{TI} formation coincided with early aberrant Ca^{2+} release (starting at ~ 1.1 seconds) and became progressively amplified during regenerative cell-wide Ca^{2+} waves (Figure 5E, bottom). We further characterized the spontaneous Ca^{2+} release from RyR2 by measuring sparks in resting cells in the presence or absence of ISO. While 1 μM ISO had a small effect on the WT cardiomyocytes, the frequency and area of Ca^{2+} sparks were dramatically increased in the ISO-treated *Ryr2^{RS/WT}* cardiomyocytes (Figure 5F: WT, $n = 6$; *Ryr2^{RS/WT}*, $n = 9$; $P < 0.05$). The increased spark areas and frequencies in *Ryr2^{RS/WT}* cells are consistent with our observation of Ca^{2+} spark fusions and repetitive activation of regenerative waves as the cause of arrhythmogenic I_{TI} (Figure 5, C and E). We conclude that an abnormal temporal and spatial increase in microscopic Ca^{2+} release events causes arrhythmogenic I_{TI} , DADs, and automaticity in *Ryr2^{RS/WT}* cardiomyocytes.

Following exercise stress testing consisting of treadmill running and EPI injection, which resulted in polymorphic VT in *Ryr2^{RS/WT}* mice ($n = 8$ of 9), hearts from WT and *Ryr2^{RS/WT}* mice were flash frozen for SR vesicle isolation for single-channel measurements in lipid bilayers. Single channels from sedentary *Ryr2^{RS/WT}* mice exhibited multiple partial opening events (subconductance states) and a low P_o at 150 nM $[\text{Ca}^{2+}]_{\text{cis}}$ simulating diastolic conditions (see also Methods; Figure 6A, left). In contrast, following stress

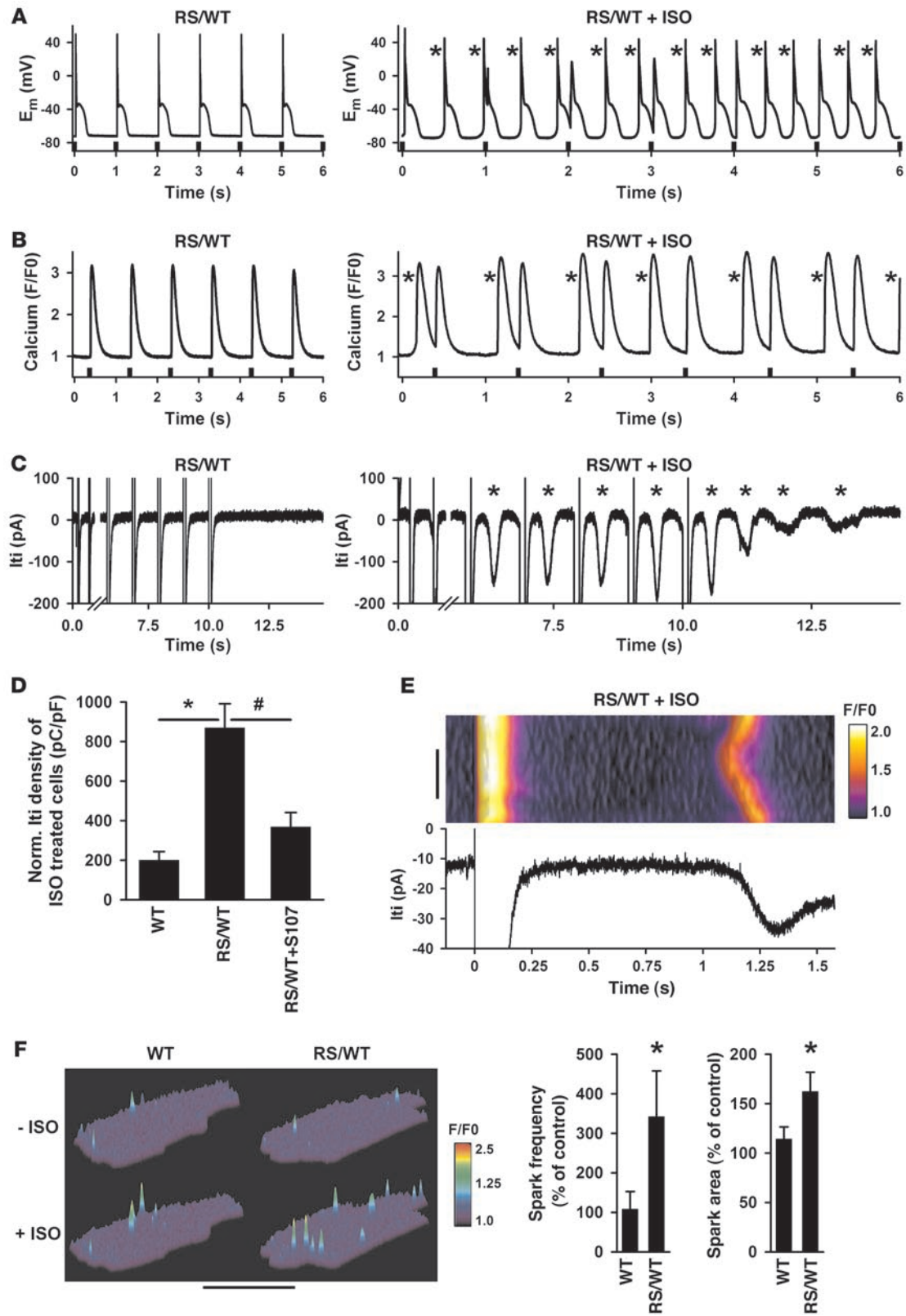




Figure 5

Electrical and Ca^{2+} cycling abnormalities in $Ryr2^{RS/WT}$ cardiomyocytes are consistent with Ca^{2+} -triggered afterdepolarizations and are reduced by the RyR2-stabilizing drug S107. (A) Representative examples of whole-cell current (E_m) recordings from $Ryr2^{RS/WT}$ cardiomyocytes paced continuously at 1 Hz (recording started after 2 minutes; pacing stimuli as indicated) under control (left) and ISO-stimulated conditions (1 μM ; right). Following ISO, aberrant membrane depolarizations (asterisks) increased in frequency and became self-sustained when pacing was stopped (not shown). (B) Intracellular Ca^{2+} transients from $Ryr2^{RS/WT}$ cardiomyocytes field-paced continuously at 1 Hz under control (left) and ISO-stimulated conditions (1 μM , right; recording started after 2 minutes continuous pacing). Aberrant spontaneous Ca^{2+} waves (asterisks) occurred irregularly and became self-sustained when pacing was stopped (not shown). (C) Representative current traces from $Ryr2^{RS/WT}$ cardiomyocytes recorded during an 0.5-Hz depolarization train in the absence (left) and presence of ISO (1 μM ; right). ISO-treated $Ryr2^{RS/WT}$ cardiomyocytes showed frequent I_{T1} (asterisks) during and after pacing. The figure illustrates currents recorded during and following the first 2 and last 5 pulses from a continuous 10-pulse (1 Hz) conditioning train. A 5.5-second-long period of the recording during the train was omitted for display purposes, and the time scale is expanded in the ISO-treated examples in the rights panels of A–C. (D) Normalized I_{T1} density in ISO-treated cells. ISO-treated $Ryr2^{RS/WT}$ cardiomyocytes ($n = 7$) showed significantly increased I_{T1} densities ($*P < 0.05$ vs. control; $n = 6$); in vivo S107 treatment significantly decreased I_{T1} density in ISO-treated $Ryr2^{RS/WT}$ cells ($*P < 0.05$; $n = 4$). (E) Simultaneous confocal Ca^{2+} imaging of a small region of interest and I_{T1} recording from an ISO-stimulated $Ryr2^{RS/WT}$ cardiomyocyte. Following regular pacing-induced Ca^{2+} release (last cycle shown on left side), intracellular Ca^{2+} and membrane current rapidly normalized to the resting (diastolic) state. $Ryr2^{RS/WT}$ cardiomyocytes showed abnormal intracellular Ca^{2+} release events, which became organized as Ca^{2+} waves, coinciding with secondary arrhythmogenic I_{T1} . Scale bar: 10 μm ; time and normalized F/F0 fluorescence signal are as indicated. (F) Representative confocal Ca^{2+} spark images from WT and $Ryr2^{RS/WT}$ cardiomyocytes before (–ISO) and after (+ISO; 1 μM) treatment. Bar graphs show significant differences ($*P < 0.05$) in average spark frequencies and average spatial area dimensions, indicating increased intracellular Ca^{2+} leak in $Ryr2^{RS/WT}$ cardiomyocytes following ISO stimulation as the subcellular origin of arrhythmogenic diastolic DADs (A), Ca^{2+} waves (B and E), and I_{T1} (C and E) events.

testing, $Ryr2^{RS/WT}$ single channels exhibited a significant increase in P_o (Figure 6A, center). One week of S107 treatment followed by stress testing resulted in redistribution of open events toward the 0-pA (closed) level (Figure 6A, right). The average RyR2 P_o was significantly increased in both EPI-treated WT and $Ryr2^{RS/WT}$ hearts. However, the P_o increase following stress testing was significantly higher in channels from $Ryr2^{RS/WT}$ hearts, indicating a gain-of-function defect (Figure 6B; $n = 7$, $P < 0.05$). Compared with those from untreated $Ryr2^{RS/WT}$ mice undergoing stress testing, RyR2 channels from S107-treated hearts showed a significantly lower P_o , comparable to that observed in RyR2 channels from sedentary mice (Figure 6B; $n = 7$, $P < 0.05$).

We have previously found significantly increased activity and calstabin2 depletion in recombinant $Ryr2$ -R2474S channels following in vitro PKA phosphorylation (22). RyR2 immunoprecipitation from cardiac homogenates followed by immunoblotting showed no change in RyR2 protein levels in WT and $Ryr2^{RS/WT}$ hearts. Exercise followed by EPI treatment resulted in similar increases in RyR2 PKA phosphorylation in WT and $Ryr2^{RS/WT}$ hearts (Figure 6, C and D). However, following stress testing, $Ryr2^{RS/WT}$ hearts revealed sig-

nificant calstabin2 depletion from the PKA-phosphorylated RyR2 complex (Figure 6E; $n = 3$, $P < 0.05$). These data are consistent with earlier in vitro experiments showing significantly decreased calstabin2 binding to recombinant homo- and heterotetrameric $Ryr2$ -R2474S channels (22). When $Ryr2^{RS/WT}$ mice were pretreated with S107 (5 mg/kg/h s.c. for 1 week) prior to stress testing, calstabin2 binding to PKA-phosphorylated $Ryr2^{RS/WT}$ cardiac channels was normalized (Figure 6E), consistent with rescue of single-channel function (Figure 6, A and B).

Discussion

We have identified leaky RyR2 channels as a mechanism underlying generalized tonic-clonic seizures and cardiac arrhythmias in heterozygous $Ryr2$ -R2474S knock-in mice. Previous studies have focused on the role of RyR2 in the heart as the cause of CPVT and SCD (13, 14, 38). Since heterozygous $Ryr2$ -R2474S mice exhibited recurrent generalized tonic-clonic seizures and electrocortical abnormalities consistent with epileptic brain activity, we propose that CPVT may actually be a neurocardiac syndrome in which patients have both neuronal seizures and exercise-induced cardiac arrhythmias that cause sudden death. Recently, we have made a second CPVT knock-in mouse ($Ryr2$ -N2386I) that also exhibits its tonic-clonic seizures and CPVT (S.E. Lehnart and A.R. Marks, unpublished data). Our data now suggest that both the cardiac arrhythmias and the seizures are likely due to the same RyR2 mutation causing a Ca^{2+} leak in the heart and the brain. Evidence for the role of the RyR2 leak as causal in the seizures is as follows: (a) $Ryr2$ -R2474S mice exhibit spontaneous and drug-induced seizures compared with WT littermate controls; (b) the seizures are inhibited by a drug, S107, that prevents RyR2 Ca^{2+} leak; the $Ryr2$ -R2474S mutation results in leaky single-channel properties of neuronal RyR2 channels examined in planar lipid bilayers; (c) seizure-like 4-AP-induced field-evoked potentials were recorded from the CA3 hippocampal region of the $Ryr2^{WT/RS}$ mice, a brain region that expresses high levels of RyR2; and (d) low Mg^{2+} and high K^+ induced aberrant Ca^{2+} signals in the CA3 hippocampal region of the $Ryr2^{WT/RS}$ mice, consistent with abnormal intracellular Ca^{2+} leak.

While seizure activity has been reported in CPVT patients with $RYR2$ and $CASQ2$ mutations (19, 20), the seizures have been attributed to arrhythmogenic cardiac dysfunction resulting in reduced blood flow to the brain (Stokes-Adams attacks) (18). However, seizures have not been documented as being associated with arrhythmias in CPVT patients (only presumed). Although the population-wide frequency of RyR2 mutations is not known (15), one postmortem study found RyR2 mutations in 14% of cases with sudden unexpected death (39). We conclude that leaky RyR2 channels may cause an inherited form of neurocardiac syndrome characterized by increased susceptibility to epilepsy and stress-induced arrhythmias in humans.

Importantly, since the arrhythmias in the CPVT mice are only observed during exercise, it is highly unlikely that neural ischemia due to repeated arrhythmias could be a cause of the seizures. Furthermore, we have shown that an RyR-specific compound, S107 (23), inhibits both the arrhythmias and the seizures. Since S107 has no effect on normal RyR channels and does not alter Ca^{2+} signaling in cells, it is highly unlikely that its protective effects against seizures has anything to do with altering generalized Ca^{2+} signaling.

Mutations in ion channel genes, including those encoding voltage-gated Na^+ and K^+ channels ($SCN1A$, $SCN1B$, $KCNQ2$, $KCNQ3$), have been linked to convulsive seizure activity (40–43). Nonsense

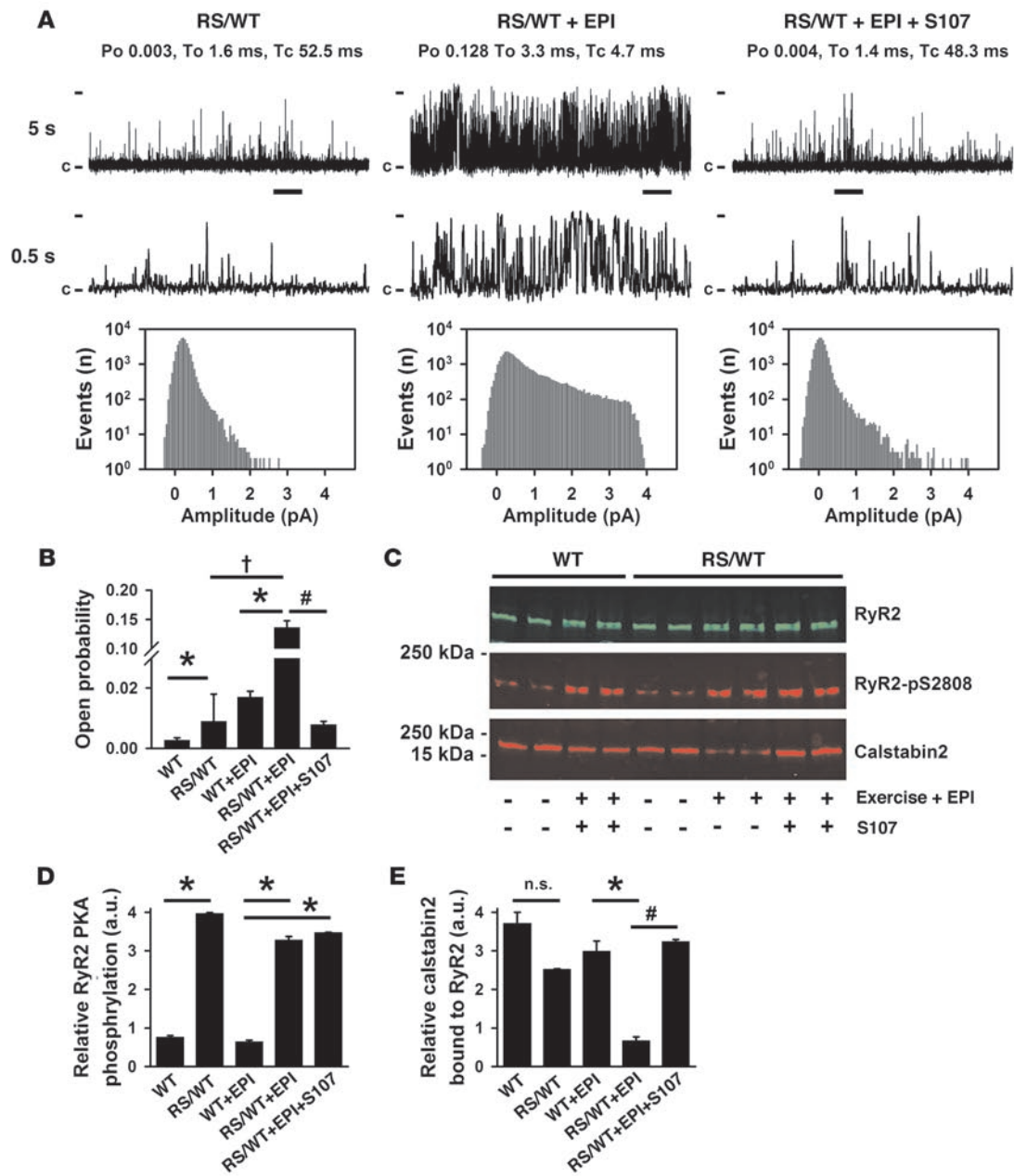


Figure 6

RyR2 channels from heterozygous *Ryr2*^{RS/WT} hearts show a gain-of-function defect that is rescued by S107 treatment. (A) Representative single-channel traces from isolated from the hearts of sedentary *Ryr2*^{RS/WT} mice (RS/WT), after maximal exercise followed by injection of 0.5 mg/kg epinephrine (RS/WT + EPI), or after 1 week treatment with S107 (5 mg/kg/h) followed by maximal exercise and EPI injection (RS/WT + EPI + S107). Thick horizontal bars below 5-second traces indicate area shown in 0.5-second traces. *P*_o, mean open (T_o) and mean (T_c) closed times, closed state (c), and fully open level (4 pA) are as indicated. Corresponding all-point histograms demonstrate altered current amplitude distribution, including multiple subconductance states and full open events in the EPI group, consistent with a gain-of-function defect. In contrast, S107-treated group histograms show redistribution toward closed states. (B) Average *P*_o of single cardiac WT and *Ryr2*^{RS/WT} channels under different treatment conditions. Single-channel measurements were performed in low activating Ca²⁺ concentrations (150 nM) to mimic diastolic conditions. **P* < 0.05 versus hearts from sedentary mice; #*P* < 0.05 versus hearts from exercise- and EPI-treated mice; †*P* < 0.05 between sedentary and EPI-treated *Ryr2*^{RS/WT} mice. Each bar represents the average of 7 channels. (C–E) Equivalent amounts of RyR2 were immunoprecipitated with an RyR2-specific antibody followed by immunoblotting: amounts of relative PKA phosphorylation of RyR2 at Ser2808 (D) and of calstabin2 bound to RyR2 (E) under the indicated conditions. Data refer to the same cardiac vesicles used in A and B. **P* < 0.05 versus hearts from sedentary mice; #*P* < 0.05 versus hearts from exercise- and EPI-treated mice.



or frameshift *SCN1A* mutations that lead to a truncated neuronal Na^+ channel α -subunit have been linked to a rare convulsive disorder, severe myoclonic epilepsy of infancy (SMEI) (41). A heterogeneous syndrome, generalized epilepsy with febrile seizures (GEFS), has been linked to both *SCN1B* and *GABAG2* mutations (44). Pharmacological seizure models have implicated abnormalities in intracellular Ca^{2+} cycling of inhibitory interneurons and/or astrocytes as a mechanism of seizure generation (1, 3), and seizures have been observed in a mouse with a partial *Ip3r1* gene deletion (3).

In the present study, we demonstrate abnormal intracellular Ca^{2+} signals in cells in the CA3 region of the hippocampus in *Ryr2^{RS/WT}* mice (Figure 3A) that are likely due to the leaky activity of the mutant RyR2 channels (Figure 3, D and E). How is intracellular Ca^{2+} linked to neuronal excitability? We speculate that intracellular Ca^{2+} leak from mutant RyR2 in brain areas (such as the hippocampus), where slow afterhyperpolarizations (AHPs) are thought to control excitability spread, may disrupt slow AHP formation during intense AP firing, which would lead to the seizure-associated altered depolarization patterns as observed in hippocampal slices. Once the identity of the cells in the hippocampus that are responsible for seizures in the *Ryr2-R2474S* mice is known it will be feasible to examine the Ca^{2+} signals in these cells in greater detail, as we have done in cardiomyocytes.

The molecular mechanisms underlying SCD, like the genetic channelopathies associated with epilepsy, have been found to involve a diverse group of ion channel mutations (15). For example, mutations in the *KCNQ1* gene have been linked to long QT syndrome type 1 (LQTS1) (15). *SCN5A* mutations have been linked to VT in LQTS3 (45) and to idiopathic ventricular fibrillation in Brugada syndrome (46). *SCN5A* is expressed in brain regions involved in epileptic activity (47), and *SCN5A* mutation carriers are prone to seizures (48–51). While it has been hypothesized that *SCN5A* mutations may cause neurogenic seizures (47), to date no supportive data have been reported.

Our data suggest that stress-induced cardiac arrhythmias are not the sole cause of seizure activity in CPVT patients. Moreover, generalized seizures result in intense stimulation of the hypothalamus and secondary activation of the sympathetic nervous system, which could lead to stress-induced arrhythmias in CPVT patients. Indeed, physical and/or emotional stresses trigger polymorphic VT and syncope in carriers of RyR2 mutations including the R2474S missense mutation investigated here (13, 14, 34). Previously, it was reported that treatment of *Ryr2-R4496C* mice with either beta blockers or JTV519 was not effective in preventing pharmacologically induced arrhythmias (37, 52). However, these studies used arrhythmia induction with pharmacological cocktails in *Ryr2-R4496C* mice (2 mg/kg EPI plus 120 mg/kg CAF i.p.) and did not address physiological mechanisms (37, 52). This pharmacologic cocktail did not involve exercise testing (followed by low-dose catecholamine EPI, 0.2–0.5 mg/kg injection), a protocol used by us (32) and others (31), and the exercise component of the protocol may be critically important in murine models of CPVT. One interpretation of the failure of the beta blockers or JTV519 to prevent pharmacologically induced arrhythmias in CPVT mice may be that the pharmacologic cocktail used in these studies could be toxic. Indeed, in the present study, S107 significantly prevented arrhythmias in *Ryr2^{RS/WT}* mice and arrhythmogenic I_{T1} in *Ryr2^{RS/WT}* cardiomyocytes.

In contrast to our previous report (32), Chen and colleagues reported no polymorphic VT in calstabin2-deficient mice (53). However, they also used only drugs without exercise testing, and

careful examination of the tracings they show following pharmacological testing show that their calstabin2-knockout mice did indeed exhibit bigeminal rhythms (53), a likely precursor of polymorphic VT/ventricular fibrillation. Our study is in agreement with other studies showing antiarrhythmic effects of the 1,4-benzothiazepine JTV519 (which is in the same class of drugs as S107 but unlike S107 is a multichannel blocker) (54–56). We have further refined these studies now by using an RyR-targeted compound, S107, which has no documented off-target activity at up to 10 μM (see supplemental data, S107 Characterization; and ref. 23). Moreover, during exercise followed by catecholamine injection, RyR2 is PKA phosphorylated at serine 2808 as we have previously reported, and mice harboring RyR2 that cannot be PKA phosphorylated (*Ryr2-S2808A* mice) are protected against stress-induced RyR2 leak (57). A recent article by Valdivia and colleagues has challenged the role of PKA phosphorylation of *Ryr2-S2808* (58); however, as we have previously noted, their study examined a mouse model of cardiac hypertrophy that is not characterized by leaky RyR2 (59).

In the present study, we found that an *Ryr2* missense mutation previously linked only to exercise-induced cardiac arrhythmias also causes generalized neuroleptic tonic-clonic seizures in mice. Based on the findings from this mouse model, we propose that an intracellular Ca^{2+} leak via defective RyR2 channels can cause both neuroleptic seizures and cardiac arrhythmias. Our data further suggest that the protective mechanism for handling a pathologic intracellular Ca^{2+} leak via defective RyR2 channels may be more robust in the heart, where arrhythmias only occur during strenuous exercise (in patients), as opposed to the brain, where seizures due to a leak via the same RyR2 channel were observed at rest (in mice). This may reflect the fact that the cardiac arrhythmias are more lethal than the neuronal seizures.

Methods

Generation of *Ryr2* knock-in mouse. The targeting vector for homologous recombination consisted of a 9.5-kb genomic DNA fragment including exons 46–54 of the RyR2 genomic sequence. The 5' and 3' flanking regions were amplified from 129SvEv mouse genomic DNA by PCR using the following 2 sets of primers: 5'-ATGCGGCCGCGCAGGAATCCTAACATCCCCTTGC-3' and 5'-TCATCGATGCACCTTATGAGATTTCTTGCCAACC-3' (5' flanking region) and 5'-TCTTAATTAACAGTAGGGACAAGAGGTTTCATCG-3' with 5'-CGTAGGAGTAAATTGTGGCTACCG-3' (3' flanking region). The resulting PCR fragments were subcloned into the pBlueScript SK- plasmid (Stratagene). Mutagenesis was performed in the 5' flanking region using the QuikChange II Site-Directed Mutagenesis Kit (Stratagene) according to the manufacturer's instructions to introduce the codon change leading to the R2474S variant in exon 49. To facilitate screening for the mutation, a conservative restriction site, BstZ17I, was introduced. The 2 arms were subsequently cloned into EcoRI and SalI sites of pACN (60). The resulting plasmid constitutes the TVR2474S targeting vector consisting of 2 arms separated by the pACN cassette. TVR2474S was linearized with AhdI and transfected by electroporation into ES cells. Transfected ES cells underwent positive selection with G418 (200 μM) for 10 days. Genomic DNA from resistant clones was analyzed for occurrence of homologous recombination by Southern blotting. Digestion of ES cell genomic DNA with BamHI followed by blotting with an external 5' probe revealed a band at 8.4 kb, indicating correct recombination as compared with 14.5 kb corresponding to the WT genotype. A 3' external probe gave an 8.1-kb band, indicating recombination, and a 14.5-kb band, indicating WT.

Recombinant ES cells were injected into C57BL/6 blastocyst-stage mouse embryos. Chimeric male mice were bred to C57BL/6 female mice



to establish a hybrid line. Germline transmission generated *Ryr2⁺Ryr2^{R2474S}* (*Ryr2^{RS/WT}*) mice. The genotypes from the F₁ and F₂ generations were determined by Southern blotting and PCR on DNA from tail biopsy specimens. Genomic DNA extracted from the tail was digested with SacI and analyzed by hybridization with an external SacI probe. The 8.0-kb band corresponds to the WT allele, whereas the 5.3-kb band corresponds to the mutant allele (Figure 1B, left). Mouse genotyping was performed using the following primers: 5'-GCTGTCCTGGAAGTACTGACTTGTA-3' and 5'-ACCCTGTGAGGCAGATAGTGC-3'. A PCR product of 819 bp was digested with BstZ171 which results in 2 specific bands at 506 bp and 313 bp from the mutant but not the WT allele (Figure 1B, right).

Anesthesia for rodent surgical instrumentation. Animals were placed on a sterile drape on a heating pad (37–38°C) under an operation microscope. All surgical instruments necessary for implantation were heat sterilized. Animals were anesthetized with 2% isoflurane (vol/vol O₂). Buprenorphine was applied once and as needed during postsurgery recovery. All protocols were reviewed and approved by the Animal Care Committee of Columbia University.

Cranial surface electrode implantation. A 10-mm midline skin incision was made on the head, and the s.c. tissue was bluntly separated. The superficial thin layer of the skull was pretreated with 10% H₂O₂ to allow for bregma and lambda landmark identification on the neurocranium for correct lead placement to assure contact with a minimum of stabilizing cement (Maxcem; Kerr). A miniature cranial socket including the EEG recording electrodes was positioned 1 mm caudal and lateral of the bregma and fixed for epidural recording from the hemispheres. Only fully recovered animals were used for EEG recording, and mice with alterations in behavior that might be related to electrode implantation were excluded from analysis. For ECG recording, a radio transmitter was implanted with electrode placement approximating the standard lead II electrical heart axis (for details, see supplemental data). Data acquisition and analysis were performed using Pinnacle software and IOX software for simultaneous ECG recordings (EMKA Technologies).

Pharmacological seizure experiments. To test for susceptibility of generalized tonic-clonic seizures, i.p. administration of freshly dissolved 4-AP (2.5 mg/kg i.p.; Sigma-Aldrich) and CAF (250 mg/kg i.p.; Sigma-Aldrich) to *Ryr2^{RS/WT}* (*n* = 8) and WT (*n* = 9) mice. A preliminary dose response trial was performed in *Ryr2^{RS/WT}* and WT mice using increasing doses of 4-AP (1.0, 2.5, 5.0, 10 mg/kg i.p.), and only 2.5 mg/kg 4-AP i.p. consistently induced minor focal symptoms (stage 1) within 60 minutes. To test for seizure susceptibility, subsequently mice were injected with 2.5 mg/kg 4-AP, followed 25 minutes later by CAF administered at a total dose of 250 mg/kg. To test for protection against seizures using S107, osmotic pumps were implanted, and mice were pretreated with S107 5 mg/kg/h for 1 week prior to seizure susceptibility testing. Phase 4 seizures associated with death could be avoided through intubation and artificial breathing, indicating diaphragm failure during sustained seizures as a potential cause of death. Mice were directly observed and videorecorded for later review and latency classification during a 60-minute observation period. All analysis of seizures were performed by an observer blinded to the experimental protocol. Mice were placed individually in Plexiglas cages before injection for video monitoring for at least 60 minutes following injection. In a different set of experiments, *Ryr2^{RS/WT}* (*n* = 6) and WT (*n* = 3) mice underwent EEG monitoring during seizure induction. Control EEG recordings were performed prior to injection. Data acquisition and analysis was performed with Pinnacle software and IOX software for simultaneous ECG recordings (EMKA Technologies). EEG activity was sampled at 1,000 Hz with a filter cutoff of 50 Hz.

Pharmacological seizure phenotype scoring. We identified 4 phases of behavioral abnormality progression within 60 minutes following i.p. drug injection, in accordance with earlier studies. Therefore, seizure activity was evaluated using a modified 4-stage classification system according to Fer-

raro et al. (61): phase 1, non-seizure activity, characterized by progressive reduction in motor activity until the animal abdomen is in full contact with cage bottom (hypoactive state); phase 2, partial or focal seizures affecting face, head, and/or forelimbs lasting 1–2 seconds; phase 3, generalized tonic-clonic seizure, with sudden loss of upright posture and whole-body clonus, including running and jumping; phase 4, maximal seizure, with tonic-clonic convulsions, followed by sudden, unexpected death.

Transmitter implantation and ECG data acquisition. Due to superior ECG quality and associated heart rhythm analysis, we used a mouse transmitter implantation procedure described by Mitchell et al. (62). After induction of anesthesia, body hair was removed from the neck and the left chest wall using a shaver and scrubbed with iodine solution. Following a 1.5- to 2-cm midline neck incision along the spine, an s.c. pocket was formed by blunt dissection. The transmitter body was sutured to the muscle just to the left of the midline, with the leads directed caudally. The cathodal lead was looped to the right within the pocket to an area overlying the right scapula and was anchored with a permanent suture. A small incision was made in the apical heart area of the left chest, and a trocar was used to tunnel s.c. along the left thoracic wall to scapula area. The anodal lead was passed through a sleeve from the back through an s.c. tunnel, and the tip of the lead was sutured to the chest wall overlying the apex of the heart; both skin incisions were then closed. The basis for this configuration was established earlier by surface electrocardiograms showing a QRS axis of approximately 72° in the frontal plane, which is oriented approximately along the axis of the implanted transmitter lead configuration (62). Electrode placement approximated an electrical heart axis similar to lead II used by standard ECG, and this specific configuration was chosen to minimize motion artifacts. Baseline and stress testing (see below) analyses were performed on recordings that were obtained at least 5 days after the implantation procedure. Twenty-four-hour recordings were analyzed off-line.

Exercise ECG test. Ambulatory ECG recordings and exercise testing were performed as described previously (32). Following 5 days of treadmill acclimatization at 24 m/min for 30 minutes, mice were exercised for at least 45 minutes on a horizontal treadmill at incrementally faster running speeds (from 12 m/min to 40 m/min), until exhaustion defined by the inability to sustain exercise at 34 m/min or greater immediately followed by epinephrine injection (0.5 mg/kg, i.p.).

Heart isolation and perfusion. All optical mapping procedures were approved by the New York University School of Medicine Institutional Animal Care and Use Committee. Heparin sodium (500 U/kg) was administered i.p. to prevent intracardiac blood coagulation. Animals were euthanized with an overdose of CO₂ and sacrificed by cervical dislocation. The hearts were quickly removed via thoracotomy and placed in Tyrode solution (130 mM NaCl, 24 mM NaHCO₃, 1.2 mM NaH₂PO₄, 1.0 mM MgCl₂, 5.6 mM KCl, 1.8 mM CaCl₂, equilibrated with a 95% O₂, 5% CO₂ gas mixture to achieve a pH of 7.4). The aorta was cannulated and Langendorff perfused at a constant pressure of 68–74 mm Hg (1–2 ml/min) at 37°C. The hearts were subsequently perfused with 1 μM di-4-ANEPPS (Molecular Probes; Invitrogen) and allowed to equilibrate for 10 minutes.

Optical mapping of murine ventricles. High-resolution optical mapping studies were performed under an upright microscope (BX-51WI; Olympus) equipped with a high-speed charge-coupled device (CCD) camera (Ultima-L; SciMedia). Excitation light from a 100-W mercury arc lamp was passed through an interference filter (530 ± 30 nm) together with a dichroic mirror (565 nm). The emitted fluorescent light was collected with a long-pass filter (>610 nm) and projected onto the CCD video camera. The recording array was 100 × 100 pixels, and data were acquired at 1,000 frames/s with 14-bit resolution. Imaging was carried out with either 2× or 4× objectives in the absence of any pharmacological or mechanical motion-reduction techniques.



Volume-conducted ECG. A bipolar electrode mounted on a micromanipulator was used to record volume-conducted electrograms from isolated hearts. Recordings were made using Ag-AgCl electrodes and placed approximately 2 mm from the heart surface. Electrograms were amplified and low-pass filtered at 300 Hz using an 8-channel Axon Instruments CyberAmp and digitally sampled at 5 kHz using the Digi-Data Corp. digitizer and the AxoScope software package (Molecular Devices). Continuous recordings were obtained through the entire experiment and stored for off-line analysis. Recordings were electronically tagged to indicate the time when optical recording was obtained.

Hippocampal slice preparation and extracellular LFP. Adult mice were anesthetized with isoflurane and decapitated and their brains quickly removed while immersed in ice-cold dissection solution. The mouse brains were fixed in agar and cut transversely at a thickness of 400 μm using a vibrating blade microtome (VT1200S; Leica). The dissection solution consisted of (in mM): 195 sucrose, 10 NaCl, 2.5 KCl, 1 NaH_2PO_4 , 26 NaHCO_3 , 4 MgCl_2 , 0.5 CaCl_2 , 10 glucose, pH 7.4 under constant 95% O_2 and 5% CO_2 bubbling. Hippocampal slices were collected in recording solution (see below) at room temperature and transferred immediately to a recording chamber, where they recovered for 2.5 hours at 32°C. Field potentials were recorded at 32°C using an interface chamber (Fine Science Tools). Slices were continuously perfused with oxygenated recording solution containing (in mM): 120 NaCl, 2.5 KCl, 1 NaH_2PO_4 , 26 NaHCO_3 , 1 MgCl_2 , 2 CaCl_2 , 10 glucose, pH 7.4 with 95% O_2 and 5% CO_2 . Low-resistance glass electrodes for extracellular recording were positioned in the proximal stratum radiatum of the CA3 subfield. To elicit epileptiform activity, 4-AP was added to the recording solution perfusate. Electrophysiological signals were amplified and filtered at 1 Hz and 10 kHz by a Cygnus Technology Inc. ER-1 Extracellular Amplifier, digitized at 2 kHz with Digidata 1440 (Molecular Devices), and stored digitally with Clampex 10.2 (Molecular Devices). Epileptiform events were analyzed using pCLAMP 10 (Molecular Devices).

Hippocampal brain slice histology. Brains were removed and snap-frozen in liquid nitrogen-cooled isopentane and included in OCT, and 10- μm sections were cut with a microtome. Cryosections were fixed in paraformaldehyde (4%), quenched in NH_4Cl (50 mM), and incubated with 2% BSA-PBS for 30 minutes at room temperature before incubation with the RyR-specific antibody (1:500; Affinity BioReagents) and following treatment with anti-mouse IgG conjugated with Alexa Fluor 488 (Invitrogen). After the coverslips were mounted in SlowFade Gold DAPI (Invitrogen), images were acquired using a parfocal fluorescence microscope (Apo-tome; Zeiss). Every other hippocampal section was stained with H&E to document normal brain cytoarchitecture and to allow for comparison with the immunostained sections in both WT and $RyR^{2RS/WT}$ (each $n = 3$).

Confocal calcium fluorescence microscopy of hippocampal brain slices. A Zeiss 5 live confocal microscope was used for intracellular Ca^{2+} imaging of hippocampal brain slices (Zeiss). Hippocampal slices were loaded for 45 minutes with the Ca^{2+} indicator Fluo-4 AM (25 μM ; Invitrogen), washed for 15 minutes, and transferred to a custom-made brain slice recording chamber on the microscope stage continuously perfused with recording solution (the same as used for field potential recording). Laser emission at 488 nm was used for excitation of Fluo-4 AM. Confocal images were acquired every 0.5 seconds. Neurons and astrocytes were distinguished on the basis of the distinct kinetics of the cellular Ca^{2+} response to high K^+ stimulation (40 mM), which was always performed at the end of the experiment. Image analysis was performed using ImageJ (<http://rsb.info.nih.gov/ij/>).

Cardiomyocyte isolation. Cardiomyocytes were enzymatically dissociated and isolated from ventricles of $RyR^{2RS/WT}$ or WT mice using a protocol modified from ref. 33. Briefly, mice were anesthetized with a ketamine/xylazine i.p. injection, and hearts were cannulated and retrogradely perfused with a dissociation buffer (DB) containing collagenase type 2 (0.5 mg/ml;

Worthington) for 7–10 minutes at 37°C, transferred into DB supplemented with Protease XIV (0.05 mg/ml; Sigma-Aldrich), and gently stirred at room temperature for an additional 8–12 minutes. Subsequently, cells were pelleted by centrifugation at 40 g for 3 minutes and resuspended in modified Tyrode solution containing BSA (5 mg/ml), and Ca^{2+} concentration was serially increased every 15 minutes, in 4 subsequent steps up to 1 mM. Cells were then plated on laminin-coated (Sigma-Aldrich) coverslips and stored at room temperature until use (1–6 hours).

Ca^{2+} imaging in cardiomyocytes. Cardiomyocytes were incubated in a 10- μM solution of Fluo-4 AM (Invitrogen) for 20 minutes at room temperature and washed in dye-free Tyrode solution for 15 minutes. Cells were plated in a perfusion chamber on the stage of a laser scanning confocal microscope (Zeiss 5 LIVE), continuously superfused with modified Tyrode containing (in mM) 130 NaCl, 4.5 KCl, 1.2 MgSO_4 , 1.2 NaH_2PO_4 , 10 HEPES, 1.2 glucose, pH 7.4, and field stimulated with 5-ms pulses at different frequencies (1–2 Hz) by programmed field stimulation (Ionoptix). ISO was freshly prepared, dissolved in Tyrode solution, and added to the cells using a separate line of the perfusion system. In a subset of cells, after stabilization of Ca^{2+} transient amplitude, stimulation was stopped, and SR Ca^{2+} load was measured by rapid CAF application (20 mM) through a local perfusion system (Picospritzer; WPI). For field-stimulated Ca^{2+} transients recording, line scan images were acquired at 500 lines/s at a typical laser power of 0.3–0.5 mW in order to minimize cell damage. For recording of sparks, cells were field stimulated at 1.0 Hz to produce steady-state conditions. Within the first 10 seconds after the last depolarization of a 15-pulse train, 80 full-frame images of 512 \times 512 pixels at a frame rate of 40 Hz were recorded, with a typical optical section of 2.1 μm and a pixel size of 0.2 μm . Images were analyzed using both ImageJ and custom-made routines based on IDL (ITT).

Electrophysiology. Action potentials and membrane currents were measured using whole-cell patch clamp with an Axopatch 200B amplifier (Axon Instruments). All measurements were obtained at room temperature (22°C). Micropipette resistance was 1.5–2.5 M Ω . The external solution used to record AP consisted of (in mM): 132 NaCl, 4.8 KCl, 10 HEPES, 5 glucose, 1.2 MgCl_2 , and 2 CaCl_2 (pH, 7.3 adjusted with NaOH). The pipette filling solution was composed of (in mM): 110 KCl, 5 ATP- Na_2 , 0.05 EGTA, 10 HEPES, 1 MgCl_2 , and 0.025 CaCl_2 (pH, 7.3 adjusted with KOH). After determination of the AP threshold by pulses of increasing voltage, APs were triggered using above-threshold 2-ms-long pulses at a frequency of 1 Hz. Voltage clamp experiments were performed using an external solution composed of (in mM): 130 NaCl, 5 CsCl, 10 HEPES, 5 glucose, 1.2 MgCl_2 , and 2 CaCl_2 (pH, 7.3 adjusted with CsOH). The pipette solution consisted of (in mM): 50 aspartic acid, 5 ATP- Na_2 , 60 CsCl, 0.1 EGTA, 10 HEPES, 1 MgCl_2 , and 0.04 CaCl_2 (pH, 7.2 adjusted with CsOH). Series of ten 100-ms-long depolarizations from -75mV to $+10\text{mV}$ at a pacing frequency of 0.5 Hz, 1 Hz, and 2 Hz were collected in the presence or absence of 1 μM ISO and followed by a 10-second pause. I_{T1} density was measured after at least 3 minutes continuous ISO perfusion, during or after the pulse protocol. In order to confirm the effect of ISO infusion, a voltage clamp protocol consisting of a first depolarization from -75mV to -40mV for 300 ms and followed by a depolarizing step from -40mV to $+10\text{mV}$ for 250 ms was used to separate I_{Na} and $I_{Ca,L}$. Data were acquired using pCLAMP 8.0 or pCLAMP 9.2 (Molecular Devices) and analyzed with SigmaPlot (SYSTAT) and Clampfit 9.2 (Molecular Devices). To simultaneously measure membrane currents and Ca^{2+} release from the SR, EGTA in the pipette filling solution was replaced with the pentapotassium salt of the Ca^{2+} dye Fluo-4 (50 μM), and voltage clamp was performed as described while acquiring images with a confocal microscope (see below).

Simultaneous recording of I_{T1} and confocal imaging of Ca^{2+} sparks and waves. For I_{T1} recording, cells were stimulated by 10 depolarizations from -75mV



to +10 mV by 100-ms-long rectangular pulses at 1 Hz in the absence and presence of ISO. To simultaneously measure I_{Ca} -induced Ca^{2+} release from the SR, Fluo-4 was excited at 488 nm, and the fluorescence was detected at 510 nm with a laser scanning confocal microscope (LSM 5 LIVE; Zeiss). Cell capacitance and I_{Ca} density were calculated with Clampex 9.0 (Molecular Devices). Global Ca^{2+} release was analyzed by routines compiled with IDL 6.0 (ITT). Myocytes were incubated with Fluo-4 AM (10 μ M) and, after a 20-minute period, were superfused with an extracellular solution containing 1.8 mM Ca^{2+} . Cells were field stimulated at 1 Hz to produce steady-state conditions. Within the first 10 seconds after the last depolarization of a 15-pulse train, spontaneous Ca^{2+} release was recorded for the next 3–4 image frames at high resolution (800 lines per frame, 1.92 ms per line) and evaluated for Ca^{2+} sparks. The recording sequence was repeated 3 times in each cell. Line scan images were analyzed, and Ca^{2+} sparks were detected off-line with a computer-based detection algorithm custom written in IDL (ITT).

Immunoprecipitation and immunoblot analysis. Brain or cardiac homogenates (100 μ g) were used to immunoprecipitate RyR channels with anti-RyR antibody (63). RyR2 was immunoprecipitated from samples by incubating 100 μ g of homogenate with anti-RyR antibody (2 μ l 5029 Ab) or RyR2-specific antibody (anti-RyR2; 1,367–1,380; generated by immunization with the RyR2-specific peptide CKPEFNHKKDYAQEK) in 0.5 ml of a modified RIPA buffer (50 mM Tris-HCl pH 7.4, 0.9% NaCl, 5.0 mM NaF, 1.0 mM Na_3VO_4 , 0.5% Triton X-100, and protease inhibitors) for 2 hours at 4°C. The samples were incubated with protein A-Sepharose beads (Amersham; GE Healthcare) at 4°C for 1 hour, after which the beads were washed 5 times with 1.0 ml RIPA. Samples were heated to 95°C and size fractionated by PAGE (6% for RyR, 15% for calstabin). Proteins were transferred to nitrocellulose membranes, and immunoblots were developed using the following antibodies: anti-calstabin (1:1,000) (22), anti-RyR (5029; 1:3,000) (63), anti-phospho-RyR2-pSer2808 (1:5,000) (64), or anti-phospho-RyR2-pSer2814 (1:5,000) (64). Protein A-Sepharose beads were added and incubated at 4°C for 1 hour. After washing 5 \times 1.0 ml with RIPA buffer, the immunoprecipitate was divided 1:4, and the proteins were size fractionated on 7.5% SDS-PAGE. All immunoblots were developed with the Odyssey

system (LI-COR Biosciences) using infrared-labeled anti-mouse and anti-rabbit IgG (1:10,000 dilution) secondary antibodies.

Single-channel recordings. RyR2 vesicle preparations were prepared from pooled isolated hippocampi ($n = 7$ brains) or isolated mouse heart ventricles. Vesicles containing native RyR2 were fused to planar lipid bilayers in 100- μ m holes in polystyrene cups separating 2 chambers. The *trans* chamber (1.0 ml), representing the intra-SR (luminal) compartment, was connected to the head stage input of a bilayer voltage clamp amplifier (Warner Instruments). The *cis* chamber (1.0 ml), representing the cytoplasmic compartment, was held at virtual ground. Symmetrical solutions used were as follows (in mM): *trans*, 250 HEPES, 53 $Ca(OH)_2$, pH 7.35; *cis*, 250 HEPES, 125 Tris, 1.0 EGTA, 0.5 mM $CaCl_2$, pH 7.35. At the conclusion of each experiment, 5 μ M ryanodine or 20 μ M ruthenium red was applied to confirm RyR2 channel identity. Single-channel data were analyzed with pCLAMP 10 software.

Statistics. Data are expressed as mean \pm SEM. ANOVA with repeated measures was used for comparison between different groups, and 2-tailed Student's *t* test was used for comparison between groups. $P < 0.05$ was accepted as significant.

Acknowledgments

This work was supported by grants from the National Heart, Lung, and Blood Institute, the American Heart Association, and the German Research Foundation (DFG).

Received for publication February 15, 2008, and accepted in revised form April 9, 2008.

Address correspondence to: Andrew R. Marks, Department of Physiology and Cellular Biophysics, BB 11-511, Columbia University College of Physicians and Surgeons, 630 W. 168th St., New York, New York 10032, USA. Phone: (212) 305-0270; Fax: (212) 305-3690; E-mail: arm42@columbia.edu.

Stephan E. Lehnart and Marco Mongillo contributed equally to this work.

1. Tian, G.F., et al. 2005. An astrocytic basis of epilepsy. *Nat. Med.* **11**:973–981.
 2. Westbrook, G.L. 2000. *Principles of neural science*. E.R. Kandel, J.H. Schwartz, and T.M. Jessell, editors. McGraw-Hill. 1414 pp.
 3. Street, V.A., et al. 1997. The type 1 inositol 1,4,5-trisphosphate receptor gene is altered in the opisthotonos mouse. *J. Neurosci.* **17**:635–645.
 4. Spacek, J., and Harris, K.M. 1997. Three-dimensional organization of smooth endoplasmic reticulum in hippocampal CA1 dendrites and dendritic spines of the immature and mature rat. *J. Neurosci.* **17**:190–203.
 5. Henzi, V., and MacDermott, A.B. 1992. Characteristics and function of $Ca(2+)$ - and inositol 1,4,5-trisphosphate-releasable stores of Ca^{2+} in neurons. *Neuroscience*. **46**:251–273.
 6. Kostyuk, P., and Verkhratsky, A. 1994. Calcium stores in neurons and glia. *Neuroscience*. **63**:381–404.
 7. Mignery, G.A., Sudhof, T.C., Takei, K., and De Camilli, P. 1989. Putative receptor for inositol 1,4,5-trisphosphate similar to ryanodine receptor. *Nature*. **342**:192–195.
 8. Holtzclaw, L.A., Pandhit, S., Bare, D.J., Mignery, G.A., and Russell, J.T. 2002. Astrocytes in adult rat brain express type 2 inositol 1,4,5-trisphosphate receptors. *Glia*. **39**:69–84.
 9. Nashef, L., Fish, D.R., Sander, J.W., and Shorvon, S.D. 1995. Incidence of sudden unexpected death in an adult outpatient cohort with epilepsy at a tertiary referral centre. *J. Neurol. Neurosurg. Psychiatry*.

58:462–464.
 10. Pedley, T.A., and Hauser, W.A. 2002. Sudden death in epilepsy: a wake-up call for management. *Lancet*. **359**:1790–1791.
 11. Rugg-Gunn, F.J., Simister, R.J., Squirrell, M., Holdright, D.R., and Duncan, J.S. 2004. Cardiac arrhythmias in focal epilepsy: a prospective long-term study. *Lancet*. **364**:2212–2219.
 12. Nashef, L., Hindocha, N., and Makoff, A. 2007. Risk factors in sudden death in epilepsy (SUDEP): the quest for mechanisms. *Epilepsia*. **48**:859–871.
 13. Priori, S.G., et al. 2001. Mutations in the cardiac ryanodine receptor gene (hRyR2) underlie catecholaminergic polymorphic ventricular tachycardia. *Circulation*. **103**:196–200.
 14. Laitinen, P.J., et al. 2001. Mutations of the cardiac ryanodine receptor (RyR2) gene in familial polymorphic ventricular tachycardia. *Circulation*. **103**:485–490.
 15. Lehnart, S.E., et al. 2007. Inherited arrhythmias: a National Heart, Lung, and Blood Institute and Office of Rare Diseases workshop consensus report about the diagnosis, phenotyping, molecular mechanisms, and therapeutic approaches for primary cardiomyopathies of gene mutations affecting ion channel function. *Circulation*. **116**:2325–2345.
 16. Lehnart, S.E., et al. 2004. Sudden death in familial polymorphic ventricular tachycardia associated with calcium release channel (ryanodine receptor) leak. *Circulation*. **109**:3208–3214.
 17. Tester, D.J., et al. 2007. A mechanism for sudden

infant death syndrome (SIDS): stress-induced leak via ryanodine receptors. *Heart Rhythm*. **4**:733–739.
 18. Leenhardt, A., et al. 1995. Catecholaminergic polymorphic ventricular tachycardia in children. A 7-year follow-up of 21 patients. *Circulation*. **91**:1512–1519.
 19. Postma, A.V., et al. 2005. Catecholaminergic polymorphic ventricular tachycardia: RYR2 mutations, bradycardia, and follow up of the patients. *J. Med. Genet.* **42**:863–870.
 20. Lahat, H., et al. 2001. A missense mutation in a highly conserved region of CASQ2 is associated with autosomal recessive catecholamine-induced polymorphic ventricular tachycardia in Bedouin families from Israel. *Am. J. Hum. Genet.* **69**:1378–1384.
 21. Mori, F., Okada, M., Tomiyama, M., Kaneko, S., and Wakabayashi, K. 2005. Effects of ryanodine receptor activation on neurotransmitter release and neuronal cell death following kainic acid-induced status epilepticus. *Epilepsy Res.* **65**:59–70.
 22. Wehrens, X.H., et al. 2003. FKBP12.6 deficiency and defective calcium release channel (ryanodine receptor) function linked to exercise-induced sudden cardiac death. *Cell*. **113**:829–840.
 23. Bellinger, A.M., et al. 2008. Remodeling of ryanodine receptor complex causes “leaky” channels: a molecular mechanism for decreased exercise capacity. *Proc. Natl. Acad. Sci. U. S. A.* **105**:2198–2202.
 24. Marks, A.R., Priori, S., Memmi, M., Kontula, K., and Laitinen, P.J. 2002. Involvement of the cardiac ryanodine receptor/calcium release channel in catecholaminergic polymorphic ventricular tachycar-



- dia. *J. Cell Physiol.* **190**:1–6.
25. Zalk, R., Lehnart, S.E., and Marks, A.R. 2007. Modulation of the ryanodine receptor and intracellular calcium. *Annu. Rev. Biochem.* **76**:367–385.
26. Maguire, C.T., et al. 2003. Implications of ventricular arrhythmia vulnerability during murine electrophysiology studies. *Physiol. Genomics.* **15**:84–91.
27. Rosembli, N., et al. 1999. Intracellular calcium release channel expression during embryogenesis. *Dev. Biol.* **206**:163–177.
28. Weiergraber, M., et al. 2006. Altered seizure susceptibility in mice lacking the Ca(v)2.3 E-type Ca²⁺ channel. *Epilepsia.* **47**:839–850.
29. Kaftan, E., Marks, A.R., and Ehrlich, B.E. 1996. Effects of rapamycin on ryanodine receptor/Ca(2+)-release channels from cardiac muscle. *Circ. Res.* **78**:990–997.
30. Noebels, J.L., and Rutecki, P.A. 1990. Altered hippocampal network excitability in the hypernoradrenergic mutant mouse tottering. *Brain Res.* **524**:225–230.
31. Mohler, P.J., et al. 2003. Ankyrin-B mutation causes type 4 long-QT cardiac arrhythmia and sudden cardiac death. *Nature.* **421**:634–639.
32. Wehrens, X.H., et al. 2004. Protection from cardiac arrhythmia through ryanodine receptor-stabilizing protein calstabin2. *Science.* **304**:292–296.
33. Lehnart, S.E., et al. 2006. Stabilization of cardiac ryanodine receptor prevents intracellular calcium leak and arrhythmias. *Proc. Natl. Acad. Sci. U. S. A.* **103**:7906–7910.
34. Priori, S.G., et al. 2002. Clinical and molecular characterization of patients with catecholaminergic polymorphic ventricular tachycardia. *Circulation.* **106**:69–74.
35. Tamaddon, H.S., et al. 2000. High-resolution optical mapping of the right bundle branch in connexin40 knockout mice reveals slow conduction in the specialized conduction system. *Circ. Res.* **87**:929–936.
36. Cerrone, M., et al. 2007. Arrhythmogenic mechanisms in a mouse model of catecholaminergic polymorphic ventricular tachycardia. *Circ. Res.* **101**:1039–1048.
37. Liu, N., et al. 2006. Arrhythmogenesis in catecholaminergic polymorphic ventricular tachycardia: insights from a RyR2 R4496C knock-in mouse model. *Circ. Res.* **99**:292–298.
38. Tiso, N., et al. 2001. Identification of mutations in the cardiac ryanodine receptor gene in families affected with arrhythmogenic right ventricular cardiomyopathy type 2 (ARVD2). *Hum. Mol. Genet.* **10**:189–194.
39. Tester, D.J., Kopplin, L.J., Creighton, W., Burke, A.P., and Ackerman, M.J. 2005. Pathogenesis of unexplained drowning: new insights from a molecular autopsy. *Mayo Clin. Proc.* **80**:596–600.
40. Wallace, R.H., et al. 1998. Febrile seizures and generalized epilepsy associated with a mutation in the Na⁺-channel beta1 subunit gene SCN1B. *Nat. Genet.* **19**:366–370.
41. Claes, L., et al. 2001. De novo mutations in the sodium-channel gene SCN1A cause severe myoclonic epilepsy of infancy. *Am. J. Hum. Genet.* **68**:1327–1332.
42. Biervert, C., et al. 1998. A potassium channel mutation in neonatal human epilepsy. *Science.* **279**:403–406.
43. Charlier, C., et al. 1998. A pore mutation in a novel KQT-like potassium channel gene in an idiopathic epilepsy family. *Nat. Genet.* **18**:53–55.
44. Baulac, S., et al. 2001. First genetic evidence of GABA(A) receptor dysfunction in epilepsy: a mutation in the gamma2-subunit gene. *Nat. Genet.* **28**:46–48.
45. Wang, Q., et al. 1995. SCN5A mutations associated with an inherited cardiac arrhythmia, long QT syndrome. *Cell.* **80**:805–811.
46. Chen, Q., et al. 1998. Genetic basis and molecular mechanism for idiopathic ventricular fibrillation. *Nature.* **392**:293–296.
47. Hartmann, H.A., Colom, L.V., Sutherland, M.L., and Noebels, J.L. 1999. Selective localization of cardiac SCN5A sodium channels in limbic regions of rat brain. *Nat. Neurosci.* **2**:593–595.
48. Juang, J.M., et al. 2003. Characteristics of Chinese patients with symptomatic Brugada syndrome in Taiwan. *Cardiology.* **99**:182–189.
49. Vincent, G.M. 2005. The Long QT and Brugada syndromes: causes of unexpected syncope and sudden cardiac death in children and young adults. *Semin. Pediatr. Neurol.* **12**:15–24.
50. Yager, M., Benson, J., and Kamajian, M. 2001. Brugada syndrome: a case study of aborted sudden cardiac death manifesting as seizures. *Crit. Care Nurse.* **21**:38, 40, 42–46.
51. Paydak, H., et al. 2002. Brugada syndrome: an unusual cause of convulsive syncope. *Arch. Intern. Med.* **162**:1416–1419.
52. Cerrone, M., et al. 2005. Bidirectional ventricular tachycardia and fibrillation elicited in a knock-in mouse model carrier of a mutation in the cardiac ryanodine receptor. *Circ. Res.* **96**:e77–82.
53. Xiao, J., et al. 2007. Removal of FKBP12.6 does not alter the conductance and activation of cardiac ryanodine receptor or the susceptibility to stress-induced ventricular arrhythmias. *J. Biol. Chem.* **282**:34828–34838.
54. Chen, Y.J., Chen, Y.C., Wongcharoen, W., Lin, C.I., and Chen, S.A. 2007. Effect of K201, a novel antiarrhythmic drug on calcium handling and arrhythmogenic activity of pulmonary vein cardiomyocytes. *Br. J. Pharmacol.* **153**:915–925.
55. Hasumi, H., Matsuda, R., Shimamoto, K., Hata, Y., and Kaneko, N. 2007. K201, a multi-channel blocker, inhibits clofilium-induced torsades de pointes and attenuates an increase in repolarization. *Eur. J. Pharmacol.* **555**:54–60.
56. Boyden, P.A., Dun, W., Barbhahiya, C., and Ter Keurs, H.E. 2004. 2APB- and JTV519(K201)-sensitive micro Ca²⁺ waves in arrhythmogenic Purkinje cells that survive in infarcted canine heart. *Heart Rhythm.* **1**:218–226.
57. Wehrens, X.H., et al. 2005. Enhancing calstabin binding to ryanodine receptors improves cardiac and skeletal muscle function in heart failure. *Proc. Natl. Acad. Sci. U. S. A.* **102**:9607–9612.
58. Benkusky, N.A., et al. 2007. Intact beta-adrenergic response and unmodified progression toward heart failure in mice with genetic ablation of a major protein kinase A phosphorylation site in the cardiac ryanodine receptor. *Circ. Res.* **101**:819–829.
59. Lehnart, S., and Marks, A.R. 2007. Regulation of ryanodine receptors in the heart. *Circ. Res.* **101**:746–749.
60. Bunting, M., Bernstein, K.E., Greer, J.M., Capecci, M.R., and Thomas, K.R. 1999. Targeting genes for self-excision in the germ line. *Genes Dev.* **13**:1524–1528.
61. Ferraro, T.N., et al. 1999. Mapping loci for pentylenetetrazol-induced seizure susceptibility in mice. *J. Neurosci.* **19**:6733–6739.
62. Mitchell, G.F., Jeron, A., and Koren, G. 1998. Measurement of heart rate and Q-T interval in the conscious mouse. *Am. J. Physiol.* **274**:H747–H751.
63. Jayaraman, T., et al. 1992. FK506 binding protein associated with the calcium release channel (ryanodine receptor). *J. Biol. Chem.* **267**:9474–9477.
64. Wehrens, X.H., Lehnart, S.E., Reiken, S.R., and Marks, A.R. 2004. Ca²⁺/calmodulin-dependent protein kinase II phosphorylation regulates the cardiac ryanodine receptor. *Circ. Res.* **94**:e61–e70.